Identifying parameters of advanced soil models using an enhanced Transitional Markov chain Monte Carlo method

Yin-Fu JIN[1], Zhen-Yu YIN[1*], Wan-Huan ZHOU[2] and Suksun Horpibulsuk[3]

Affiliation:

1 Department of Civil and Environmental Engineering, The Hong Kong Polytechnic University, Hung Hom, Kowloon, Hong Kong, China

2 State Key Laboratory of Internet of Things for Smart City and Department of Civil and Environmental Engineering, University of Macau, Macau S.A.R., China

3 School of Civil Engineering, Suranaree University of Technology, Muang District, Nakhon Ratchasima, Thailand

* Corresponding author: Dr Zhen-Yu YIN, Tel: +33 (0)240371588 / Fax: +33 (0)240372535; E-mail: zhenyu.yin@polyu.edu.hk; zhenyu.yin@gmail.com

Abstract: Parameter identification using Bayesian approach with Markov Chain Monte Carlo (MCMC) has been verified only for certain conventional simple constitutive models up to now. This paper presents an enhanced version of the Differential Evolution Transitional MCMC (DE-TMCMC) method and a competitive Bayesian parameter identification approach for applying to advanced soil models. To realise the intended computational savings, a parallel computing implementation of DE-TMCMC is achieved using the Single Program/Multiple Data (SPMD) technique in MATLAB. To verify its robustness and effectiveness, synthetic numerical tests with/without noise and real laboratory tests are used for identifying the parameters of a critical state–based sand model based on multiple independent calculations. The original TMCMC are also used for comparison to highlight that DE-TMCMC is highly robust and effective in identifying the parameters of advanced sand models. Finally, the proposed parameter identification using DE-TMCMC is applied to identify parameters of an elasto-viscoplastic model from two in situ pressuremeter tests. All results demonstrate the excellent ability of the enhanced Bayesian parameter identification approach on identifying parameters of advanced soil models from both laboratory and in situ tests.

Key words: Bayesian parameter identification; Transitional Markov chain Monte Carlo; constitutive model; sand; clay; pressuremeter

1 Introduction

Constitutive models play an important role in geotechnical engineering and can be classified as (1) linear-elastic model, (2) elastic perfectly plastic models (such as the Mohr-Coulomb), (3) nonlinear models (such as hardening soil model [1], nonlinear Mohr-Coulomb [2,3]), (4) critical-state-based advanced models (such as the modified cam-clay model [4]; Nor-Sand model [5]; CSAM model [6]; Severn–Trent model [7]; UH models [8-11]; SANISAND model [12]; SIMSAND model [13,14,2]; ANICREEP model [15,16]), hypoplasticity models [17-19,3,20,21], and (5) micromechanical models [22-28]. The last two categories are usually called advanced soil models, and such models have allowed the garnering of increasingly accurate and reliable descriptions of state-dependent mechanical behaviours of soils, resulting in complexities as well as some additional parameters. The accuracy of parameters of a model significantly influences its modelling performance and can even result in inaccurate predictions [29-35]. Accordingly, parameter identification is a vital issue surrounding the application of advanced constitutive models in geotechnical engineering.

Yin et al. [36] distinguished three approaches of parameters determination from experimental data: analytical methods, empirical correlations and inverse analysis methods. Among them, inverse analysis produces a relatively objective determination of the parameters for an adopted soil model, even for those without direct physical meaning, and thus has been widely adopted. The key methods of inverse analysis are divided into two categories: (1) deterministic methods and (2) probabilistic methods. Deterministic methods merely focus on finding a set of fixed values for the input parameters of concern [13,14,2,37,35,36,38-42] without taking into account the variability and uncertainty of soils. By contrast, probabilistic methods are competitive because of their consideration of uncertainty. Of these, the Bayesian approach to parameter identification has been applied in different fields [43-62] in which parameters of concern have been treated as random variables and expressed in terms of posterior distributions and statistics. Up to now, such applications have involved only certain conventional simple soil models (e.g., the linear elastic model [54], the one-dimensional elasto-plastic model [53], the Hardening Soil model [45]), whereas parameter

identification involving advanced constitutive models (e.g., critical state–based models) has rarely been reported – hence this investigation.

When conducting Bayesian parameter identification, the Markov chain Monte Carlo (MCMC) simulation is generally known for its ability to efficiently derive a posterior distribution [51,52,63,48,64,65]. The adopted MCMC highly governs the performance of identified parameters in terms of accuracy and reliability. MCMC sampling (e.g., Metropolis–Hastings algorithm [66]) produces samples that are statistically dependent, possibly reducing the efficiency of statistical estimators, and indeed most of them become inefficient when the number of variables is large [67]. In seeking to overcome such issues, the transitional MCMC (TMCMC) proposed by Ching and Chen [68] has proved to be more efficient for high-dimensional problems [69-72,67,68]. Evidently, such efforts have improved the performance of MCMC, but some observations have indicated that the posteriors estimated using the TMCMC tend to fall into local convergence when solving certain problems [67]. Accordingly, further improvement of TMCMC for Bayesian parameter identification is necessary, especially for advanced soil models.

This paper aims to develop an efficient approach to Bayesian parameters identification for advanced soil models through the enhancement of TMCMC. To this end, Bayesian parameter identification is first introduced in principle. To improve the performance of TMCMC, a differential evolution–Markov chain algorithm is implemented in the process of new samples. To save on computational costs, a parallel computing implementation of DE-TMCMC is achieved using the Single Program/Multiple Data (SPMD) technique in MATLAB. The enhanced DE-TMCMC based parameter identification approach is validated by identifying parameters of a critical state–based sand model from synthetic numerical tests with/without noise first and then from real laboratory tests. Finally, an application of the proposed approach to an elasto-viscoplastic clay model based on two in situ pressuremeter tests is presented.

2 Enhanced DE-TMCMC based Bayesian identification with parallel computing

2.1 Framework of Bayesian parameter identification

According to Yuen [73], the Bayesian approach can update model parameters and characterize uncertainties using their posterior probability distribution functions (PDFs).

Following a Bayesian formulation [74,75,73] and assuming that the observation data and the model predictions satisfy the prediction error equation, the observation can be expressed as:

$$U_{\text{obs}} = c \cdot U_{\text{num}}(\mathbf{b}) \tag{1}$$

where $\mathbf{b}$ is a vector of model parameters; $c \sim N(1, \sigma_\varepsilon^2)$ are a one-mean Gaussian random variable with variance σ_ε^2 that represents the prediction error variance, and this σ_ε is an unknown parameter in addition to the soil model parameters $\mathbf{b}$.

Uncertainties of parameters can be evaluated using the posterior PDFs, with the expression of the posterior PDF for data D written as follows:

$$p(\boldsymbol{\theta}|D) = \frac{p(\boldsymbol{\theta})\, p(D|\boldsymbol{\theta})}{p(D)} \tag{2}$$

where $\boldsymbol{\theta}=[\mathbf{b}, \sigma_\varepsilon]$ is the uncertain parameters; $p(D)$ is the evidence; $p(\boldsymbol{\theta})$ is the prior PDF of the uncertain parameters $\boldsymbol{\theta}$, which is based on the previous knowledge or user's judgment; and $p(D|\boldsymbol{\theta})$ is the likelihood function expressing the level of data fitting. If the prediction errors in different measured data are statistically independent, then the likelihood function can be computed as follows [76-78]:

$$p(D|\boldsymbol{\theta}) = \left(2\pi\sigma_\varepsilon^2\right)^{-\frac{N}{2}} \exp\left[-\frac{N}{2\sigma_\varepsilon^2} J_g(\mathbf{b}; D)\right] \tag{3}$$

where N is the number of measured data and $J_g(\mathbf{b}; D)$ is the goodness-of-fit function representing the degree of data fitting. For reasons of numerical stability and algebraic simplicity it is often convenient to work with the log-likelihood. Accordingly, the log-likelihood $\ln p(D|\boldsymbol{\theta})$ is expressed as:

$$\ln p(D|\boldsymbol{\theta}) = -\frac{N}{2}\ln\left(2\pi\sigma_\varepsilon^2\right) - \frac{N}{2\sigma_\varepsilon^2} J_g(\mathbf{b}; D) \tag{4}$$

Generally, deformation and stress are two extremely important indicators for soil behaviours. The measurement produced by a laboratory test usually contains two curves, such as the curves ε_a–q and ε_a–e for the drained triaxial test or the curves ε_a–q and ε_a–u for the undrained triaxial test (where ε_a is axial strain, q is deviatoric stress, e is void ratio, and u is excess pore water pressure).

Accordingly, a goodness-of-fit function involving these two important indicators is reasonable. According to Jin et al. [13,2], a normalized goodness-of-fit function is adopted due to the error independent of the magnitude of different variables (e.g., q and e or u), which is expressed as:

$$J_g\left(\mathbf{b};D\right)=\frac{1}{N_0 N}\sum_{j=1}^{N_0}\left[\sum_{i=1}^{N}\left(\frac{U_{\text{obs}}^{i}-U_{\text{num}}^{i}}{U_{\text{obs}}^{i}}\right)^2\right]_j \tag{5}$$

where N is the number of measured values, N_0 is the number of curves for one test, U_{obs}^{i} is the value of measurement point i, and U_{num}^{i} is the value of calculation at point i.

With multiple observations and types of observations, likelihood values for each observation must be combined into an overall value for each candidate parameter set [79]. When the measured data D involve M tests during Bayesian parameter identification, the likelihood function is expressed as:

$$\ln p\left(D|\boldsymbol{\theta}\right)=\sum_{i=1}^{M}\mathrm{w}_i \ln p\left(D_i|\boldsymbol{\theta}\right) \tag{6}$$

where M is the number of involved tests, $\mathrm{w_i}$ is weight of $p\left(D_i|\boldsymbol{\theta}\right)$, and $p\left(D_i|\boldsymbol{\theta}\right)$ is the likelihood corresponding to the test i. In this study, the weight of each likelihood for all involved tests is considered the same and thus equal to 1.

Because the soil model involves high-dimensional nonlinear functions, the posterior $p\left(\boldsymbol{\theta}|D\right)$ must be evaluated numerically, such as by the TMCMC method. The posterior PDF $p\left(\boldsymbol{\theta}|D\right)$ represents the updated belief about the parameter vector $\boldsymbol{\theta}$ after obtaining the evidence of D. An accurate estimator of the parameters $\boldsymbol{\theta}$ for the adopted soil model is the Maximum a Posteriori (MAP) estimation. The MAP parameter vector $\boldsymbol{\theta}_{\text{MAP}}$ can be computed as follows:

$$\boldsymbol{\theta}_{\text{MAP}}=\arg\max p\left(\boldsymbol{\theta}|D\right)=\arg\max\frac{p\left(\boldsymbol{\theta}\right)p\left(D|\boldsymbol{\theta}\right)}{p\left(D\right)} \tag{7}$$

where the arg max is to find the points within a domain for a given function at which the function values are maximized.

2.2 Proposition of enhanced DE-TMCMC

The TMCMC method was originally developed by Ching and Chen [68] as a combination of the sequential particle filter method [80] and MCMC. The method begins with the prior distribution $p(\boldsymbol{\theta})$ and makes a gradual transition to the posterior by optimization at each round of samplings. The key idea of TMCMC is that of proposal density, which corresponds to the j^{th} round of sampling $p(\boldsymbol{\theta})_j$ determined as,

$$p(\boldsymbol{\theta})_j \propto p(\boldsymbol{\theta}) \cdot L(\boldsymbol{\theta}|D)^{q_j} \tag{8}$$

where $q_j \in [0, 1]$ is chosen following $q_0=0< q_1<...< q_m=1$ with $j=0, 1, \ldots, m$ denoting the stage level. Consequently, $p(\boldsymbol{\theta})_0$ equals the prior distribution $p(\boldsymbol{\theta})$ for $j=0$, and $p(\boldsymbol{\theta})_m$ is the posterior distribution $p(\boldsymbol{\theta}|D)$ for $j=m$.

Details about execution of the TMCMC algorithm can be found in Ching and Chen (2007) [68]. In this study, only certain key steps are summarized:

1. Calculate the q_j. If $q_j>1$, then set $q_j=1$.

2. For all samples $k=1, 2, \ldots, N_s$, compute a weighting coefficient $w_{j,k}$:

$$w_{(j,k)}=\left[L\left(\boldsymbol{\theta}_{(j-1,k)}|D\right)\right]^{q_j-q_{j-1}} \tag{9}$$

3. Compute the mean of the weighting coefficient

$$S_j = \frac{1}{N_s}\sum_{k=1}^{N_s} w_{(j,k)} \tag{10}$$

4. Compute the covariance matrix of the Gaussian proposal distribution

$$\boldsymbol{\Sigma}_j = \beta^2 \cdot \sum_{k=1}^{N_s}\left[\frac{w_{(j,k)}}{S_j N_s}\left(\boldsymbol{\theta}_{(j-1,k)}-\bar{\boldsymbol{\theta}}_j\right)\cdot\left(\boldsymbol{\theta}_{(j-1,k)}-\bar{\boldsymbol{\theta}}_j\right)^T\right] \tag{11}$$

with

$$\bar{\boldsymbol{\theta}}_j = \frac{\sum_{l=1}^{N_s} w_{(j,l)}\boldsymbol{\theta}_{(j-1,l)}}{\sum_{l=1}^{N_s} w_{(j,l)}} \tag{12}$$

5. For each l in $[1,\ldots, N_s]$, set $\boldsymbol{\theta}^c_{(j,l)}=\boldsymbol{\theta}_{(j-1,l)}$. Then for $k=1, 2, \ldots, N_s$, do the following MCMC sampling:

5.1 Select the index l from the set [1, 2, …, N_s] using the sequential importance sampling (SIS) method, where each l is assigned probability $w_{(j,l)} \Big/ \sum_{n=1}^{N_s} w_{(j,n)}$.

5.2 Propose a new sample: Draw $\boldsymbol{\theta}^c$ *from the normal distribution* $N(\boldsymbol{\theta}_{(j,l)}^c, \boldsymbol{\Sigma}_j)$.

5.3 The remaining steps are identical to those in the Metropolis algorithm.

6. If q_j=1, then stop the iteration; otherwise set $j=j+1$ and continue the above process.

The details of the original TMCMC method, with its MATLAB code, can be found in Ching and Chen [68].

To improve the performance of original TMCMC, a differential evolution–Markov chain algorithm proposed by Vrugt [81] was adopted in this study to replace the process that proposes a new sample in step 5.2, which can be generated as:

$$\boldsymbol{\theta}_{(j,l)}^{\text{new}} = \boldsymbol{\theta}_{(j,l)}^{c} + d\boldsymbol{\theta}_{(j,l)} \tag{13}$$

with

$$d\boldsymbol{\theta}_{(j,l)} = (1+\lambda)\cdot\gamma\cdot\left[\left(\boldsymbol{\theta}_j^{best} - \boldsymbol{\theta}_{(j,l)}^{c}\right) + \left(\boldsymbol{\theta}_{(j,a)} - \boldsymbol{\theta}_{(j,b)}\right)\right] + \zeta \tag{14}$$

where $\boldsymbol{\theta}_{(j,l)}^{\text{new}}$ is the new sample; $\boldsymbol{\theta}_{(j,l)}^{c}$ is the current sample; $\boldsymbol{\theta}_j^{best}$ is the sample corresponding to the maximum weight in the current iteration; d is the dimension of $\boldsymbol{\theta}$; $\boldsymbol{\theta}_{(j,a)}$ and $\boldsymbol{\theta}_{(j,b)}$ are two vectors consisting of d variables, where the indices a and b are two integers drawn from [1,…, N_s]; $\gamma = 2.38/\sqrt{2\delta d}$ is the jump rate; δ denotes the number of chain pairs used to generate the jump with a default value of δ=3 according to Vrugt [81]. The values of λ and ζ are sampled independently from the uniform distribution [$-c$, c] and the normal distribution $N(0, c^*)$, respectively. In this study, the c=0.1 and $c^*=10^{-12}$ were employed, as recommended by Vrugt [81].

After differential evolution, a binomial crossover operation forms the final sample,

$$\boldsymbol{\theta}_{(j,l)}^{\text{new}} = \begin{cases} \boldsymbol{\theta}_{(j,l)}^{\text{new}}, & \text{if rand}(0,1) \le CR \text{ or } l = l_{rand} \\ \boldsymbol{\theta}_{(j,l)}^{c}, & \text{otherwise} \end{cases} \tag{15}$$

where rand(0, 1) is a uniform random number within [0, 1]; l_{rand}=randint (1, d) is an integer randomly chosen from 1 to d and is newly generated for each l; the crossover probability $CR \in [0, 1]$

corresponds roughly to the average fraction of the vector components that are inherited from the mutation vector, with *CR*=0.9 taken in this study.

For simplicity's sake, the original TMCMC is referred as "O-TMCMC," and the enhanced TMCMC as "DE-TMCMC" in the following sections.

2.3 Parallel computing DE-TMCMC

Stochastic simulation algorithms, such as the TMCMC algorithm, used in Bayesian inverse modelling require numerous simulation runs when used for geotechnical engineering problems. For large-order computational models, the computational demands involved in the TMCMC sampling algorithm are excessive, sometimes to the point of being unacceptable. Accordingly, high-performance computing (HPC) techniques are vital for their ability to reduce computation time. Most MCMC algorithms involve a single Markov chain and are thus not parallelizable. Hence parallel computing algorithms should be implemented for use with the enhanced DE-TMCMC algorithm, efficiently distributing computations on multicore CPUs [82,83].

In this study, the SPMD (Single Program/Multiple Data) technique in MATLAB was adopted to achieve a parallel computing implementation of DE-TMCMC. Typical applications appropriate for SPMD are those that require simultaneous execution of a program on multiple data sets when communication or synchronization is required between the workers. The SPMD efficiently distributes the computations involved in the DE-TMCMC algorithm to available heterogeneous GPUs and multi-core CPUs so that the number of log-likelihood evaluations is the same for each computer worker. The SPMD technique is computationally efficient when the computational time for a log-likelihood evaluation is the same independent of the location of sample in the parameter space. More information about the SPMD technique can be found in the MATLAB manual.

Fig. 1 shows the parallel computing strategy in DE-TMCMC using the SPMD technique, where log-likelihood represents the user-defined function for computing the log-likelihood; *N*_workers is the total number of computer workers (e.g., 8 for a 4-cores CPU) and "labindex" is the index of computer workers, automatically identified in MATLAB. The entire calculation will be distributed among different computer workers according to the value of labindex. Note that the number of

samples N_s should be an integer multiple of the number of computer workers, N_workers, in parallel computation.

Not surprisingly, drastic reductions of time can be achieved using this parallel implementation of the DE-TMCMC algorithm. Furthermore, the time savings differ for the same case on different computers with different settings: powerful computers with many multi-core CPUs can save more computational time.

3 Performance of parallel computing DE-TMCMC

In order to assess the efficiency of the parallel computing DE-TMCMC methodology for the identification of parameters of advanced constitutive models, several MCMC simulations were carried out using the O-TMCMC and DE-TMCMC respectively for a comparison on synthetic data and real experimental data. The following cases were considered:

(1) Identifying parameters of SIMSAND model (see Appendix) from synthetic test data for the numerical validation;

(2) Identifying parameters of SIMSAND model from real experimental data for the applicability.

3.1 Numerical validation on synthetic laboratory tests

To generate the synthetic tests, a set of typical parameters of SIMSAND model were adopted, as summarized in Table 1. Using these values, three synthetic drained triaxial tests (e_0=0.6 and p'_0=800 kPa, e_0=0.7 and p'_0=200 kPa, e_0=0.8 and p'_0=25 kPa) were computed. Note that the stain measurement (e.g., linearized strain suitable for small strain, logarithmic strain suitable for large strain) may influence the obtained parameters such as stiffness or critical state related parameters, depending on their contributions to the material model. In these synthetic tests only the linearized strain measurement was used as usually adopted in analysing laboratory tests (e.g. Verdugo and Ishihara [84]). According to Jin et al. [2], tests with wider range of confining stress involved in parameter identification would be helpful on finding the accurate CSL. To increase the difficulty of evaluation, the computed stress and void ratio of three tests were contaminated by additive Gaussian noise with standard deviation 0.1. Adding Gaussian noise to synthetic data is a relatively intuitive and quantitative approach for investigating this problem. The purpose of this adding Gaussian noise

is to show the anti-interference ability of the proposed algorithm in parameter identification. The results of three synthetic drained tests without/with noise are shown in Fig. 2.

For both cases, 2000 samples per stage was implemented, and thus 2000*m (m representing total number of stages in TMCMC) samples were totally generated in TMCMC simulation. According to previous studies [71,68,72,67,78], the total number of stages for different cases were not always the same. The prior PDF of all uncertain parameters was assumed to follow a multivariable uniform distribution. These were independently uniformly distributed within the lower and upper bounds. The bounds of each prior PDF for all parameters are summarized in Table 1. In this case, the Poisson's ratio υ, bulk modulus K_0 and nonlinear elasticity parameter n were fixed. The remaining parameters of SIMSAND along with the uncertainty σ_ε were identified using the Bayesian parameter identification, adopting O-TMCMC and DE-TMCMC, respectively. Note that both O-TMCMC and DE-TMCMC were enhanced with the parallel computing technique to save the computational costs.

For both TMCMC simulations, ten independent runs were performed to avoid the randomness in order to show the performance of the proposed DE-TMCMC. For Bayesian analysis, the generated samples should be represented by the "entire" PDF to evaluate the performance of adopted approaches. However, commonly the multidimensional distribution over all the space of unknown parameters cannot be directly illustrated due to its high dimension. Thus, the obtained posterior PDF of each parameter was presented by mean and standard deviation values for a convenient comparison between O-TMCMC and DE-TMCMC. Fig. 3 and Fig. 4 show the mean values of all parameters and the uncertainties for DE-TMCMC and O-TMCMC on synthetic data without/with noise, respectively. Regardless of whether the used data is noisy, the parameters identified by DE-TMCMC in comparison to O-TMCMC fluctuate slightly, and basically stabilize to a constant value among multiple calculations, demonstrating the excellent performance of the proposed DE-TMCMC on attaining the robustness.

A good MCMC method is not only robust but also effective that the concerned parameters should be exactly identified. The presented results in Fig. 3 also show that the value of each parameter identified by DE-TMCMC is closer to the true value than the one identified by

O-TMCMC on synthetic data without noise, which indicates the effectiveness of the proposed DE-TMCMC. Moreover, as shown in Fig. 4, the similar exact parameters can also be identified by DE-TMCMC even though the used data is noisy, which indicates the outstanding anti-interference capability of the DE-TMCMC. Thus, the DE-TMCMC is more suitable and reliable than O-TMCMC when identifying the parameters for advanced sand models from noisy data. Furthermore, besides the MAP values of parameters of SIMSAND, the uncertainties of used data can also be exactly identified by DE-TMCMC, as shown in Fig. 3(i) and Fig. 4(i). However such uncertainty is overestimated by O-TMCMC. This comparison demonstrates the reliability of DE-TMCMC when identifying the uncertainty of practical observations.

Table 1 summarizes the average MAP values of SIMSAND parameters identified by DE-TMCMC. Except three CSL-related parameters (e_{ref}, λ and ξ), others approximately equal to the true values. Fig. 5 shows the comparison of CSL computed by the parameters identified by DE-TMCMC from the data without/with noise. Slight difference between three CSLs is found at the stress level ranging from 100 to 1000 kPa. Using the MAP parameters, three drained triaxial tests were simulated by SIMSAND, as shown in Fig. 6. Good agreement between simulations and synthetic data first shows that the identified parameters are accurate, and secondly, although the parameters of CSL are inaccurate, the impact on simulation results is not significant.

Overall, the proposed DE-TMCMC is superior to O-TMCMC in identifying parameters of advanced sand model in terms of robustness, effectiveness and reliability regardless of whether the used data is noisy or not.

3.2 Performance on real laboratory tests

3.2.1 Laboratory tests of Toyoura sand

A series of drained triaxial tests performed on Toyoura sand by Verdugo and Ishihara [84] was selected for this case. Toyoura sand is a uniform fine quartzitic sand consisting of sub-rounded to sub-angular particles having a mean grain size d_{50}=0.17 mm and a uniformity coefficient $C_u=d_{60}/d_{10}$=1.7. The minimum and maximum void ratios are e_{min}=0.597 and e_{max}=0.977.

The initial void and confining pressure for each test is summarized in Table 2. The experimental results for all triaxial tests are shown in Fig. 7. To form a comprehensive group of experiments that

can well reflect the common sand behaviours, following the recommendation of Jin et al. [2], three triaxial tests (one drained (test 2) and two undrained (tests 7 and 12)) were selected as objectives for parameter identification. Other remaining tests were used to assess the accuracy of obtained parameters.

In this study, the Poisson's ratio υ was assumed to be 0.2, a common value for most sands. Except for the Poisson's ratio (υ), the remaining parameters of SIMSAND along with the uncertainty σ_ε were identified using DE-TMCMC combining with Bayesian method.

3.2.2 Results and discussions

Similarly, this case also independently ran 10 times to avoid randomness. To show the effectiveness of the proposed DE-TMCMC in identifying parameters of sand model, the identification of parameters was also conducted by optimization techniques [36,13] for comparison. The obtained parameters are summarized in Table 3. Although the optimization based identification does not take the soil uncertainty into account, the results can be deemed a set of reference values to assess the effectiveness of the proposed DE-TMCMC: a closer distance between the solution of optimization and generated samples of MCMC means more reliable parameters achieved, indicating a more effective MCMC method adopted or developed.

Fig. 8 compares the mean values of each parameter and the uncertainty for two approaches under multiple calculations. Similar phenomenon that the parameters identified by DE-TMCMC fluctuate slightly is found. In contrast, the results of O-TMCMC are unsatisfactory with large fluctuations, which obviously demonstrate the bad robustness of O-TMCMC, especially for the friction angle ϕ_μ which should be almost constant for a given granular material. Except three CSL-related parameters, other parameters identified by DE-TMCMC are very close to the reference values compared to O-TMCMC. The reason leading to the inaccurate CSL is also the small stress range of test involved in the parameter identification. Without considering this, the comparison between DE-TMCMC and O-TMCMC demonstrates that the DE-TMCMC is robust and effective in identifying parameters of SIMSAND from real laboratory tests.

Fig. 9 shows the values of standard deviation of each parameter and the uncertainty for two approaches. Large fluctuation in data of standard deviation indicates the instability of posterior PDF.

Furthermore, the large value of standard deviation means the generated samples distribute in a large range, implying the existence of local convergence. For granular material, the friction angle ϕ_μ is a key parameter relating to material strength. In SIMSAND, the plastic modulus k_p and dilatancy-related parameters A_d and n_d are key parameters relating to material deformation. Thus the accuracy of ϕ_μ, k_p, A_d and n_d can be an indicator of the effectiveness of DE-TMCMC. The evolutions of four selected parameters corresponding to the larger standard deviation at final stage with q_j=1 for O-TMCMC and DE-TMCMC were plotted. For ϕ_μ and k_p, the comparisons at the calculations 2^{th}, 3^{th}, 6^{th}, and 10^{th} are shown in Fig. 10. Fig. 11 shows the comparison of evolutions at final stage for A_d and n_d. For DE-TMCMC, the parameters gradually converge to a narrow range from the prior uniform distribution. However, for O-TMCMC, the identification falls into local convergence and thus results in unreasonable values of ϕ_μ, k_p, A_d and n_d for Toyoura sand [13,12]. In contrast, this situation is overcome by DE-TMCMC with a domain of more reliable parameters. All comparisons demonstrate that the proposed DE-TMCMC is robust and can overcome the problem of local convergence for parameter identification of advanced soil models.

The average MAP parameters and the standard deviation of posterior PDF–identified by O-TMCMC and DE-TMCMC – are also summarized in Table 3. The MAP parameters identified using DE-TMCMC are more close to those obtained by Taiebat and Dafalias [12] and Jin et al. [13], which indicates that the parameters obtained by DE-TMCMC are more reasonable and reliable than those by O-TMCMC. Furthermore, finding the uncertainty of parameters is also important compared to the MAP values, which is the characteristic of Bayesian approach unlike the deterministic methods. The uncertainty of obtained parameters can be used to assess the uncertainty of predictions. Therefore, using all obtained 2000 samples, the uncertainty of predictions for two used approaches was compared by error bar plot, as shown in Fig. 12 on objective tests 2, 7 and 12. In fact, the outstanding predictive ability of SIMSAND model that can well capture the behaviour of Toyoura sand is known before conducting this case [13,85]. Thus, it seems that the O-TMCMC overstates the uncertainty of predictions compared to the proposed DE-TMCMC, indicating that the proposed DE-TMCMC is more effective than O-TMCMC in terms of the reliability of identified parameters. To demonstrate the performance of the MAP parameters identified by DE-TMCMC, a series of

predictions were conducted, as shown in Fig. 13. Good agreement can be found between the numerical predictions and experiments, demonstrating the rationality of the parameters obtained by the Bayesian parameter identification with DE-TMCMC.

Furthermore, the test results sometimes are not consistent themselves, which is probably caused by: (a) an inherent spatial variability of soil properties, (b) experimental uncertainty (measurement scatter) due to limitations of the experimental techniques and (c) sampling uncertainty (statistical uncertainty) due to the limited number of soil samples used in the investigation. Such inconsistency would lead to variability of parameters for model of interest, which can be quantified by the proposed Bayesian approach with DE-TMCMC from available experimental data. In practice, such inconsistency (experimental and sampling uncertainties) can be incorporated into probabilistic analyses using random field methods, such as by the approach developed by David Mašín [86].

Overall, through the above comparisons, the enhanced DE-TMCMC is highly robust and efficient in identifying the parameters of advanced soil models.

4 Application to in-situ testing

4.1 Identifying parameters from pressuremeter test

To evaluate the performance of Bayesian parameter identification in conjunction with the DE-TMCMC through use of in situ testing, two self-boring pressuremeter (SBP) tests performed in the Burswood Peninsula site at a depth of 5.25 m by Lee and Fahey [87] were selected as the objectives. A two-dimensional finite element model, with boundaries in an axisymmetric condition to simulate the pressuremeter, was created in a commercial finite element code ABAQUS, as shown in Fig. 14. The upper and bottom sides were fixed only for vertical displacement, whereas the right side was fixed for horizontal displacement. The loading could then be generated by applying horizontal displacement at the left side. Accordingly, the horizontal displacement had its biggest value at the left side and gradually decreased to zero as it reached the right side. Altogether, 240 four-node reduced-integration elements (CAX4RP) were used to simulate the soil. The same displacement seen in a typical field test was applied, and at each step, the same displacement increment was applied.

For the two tests, the expansion phase was conducted at two different rates up to around 10 % of the cavity strain: 0.167 %/s and 0.0185 %/s, respectively. The initial effective vertical stress σ'_{v0}

was 31 kPa, and the lateral earth coefficient K_0 was 0.9, where the initial value of vertical stress is estimated from the effective unit weight of soils with the depth, and the horizontal stress relating to the earth pressure coefficient is measured as the initial value of lateral stress from test results according to the site investigation and two SBP tests conducted by Lee and Fahey [87]. The water pore pressure was 38.8 kPa. In this case, the elasto-viscoplastic model ANICREEP was adopted to simulate the rate-dependency behaviour of soft clay. More details of ANICREEP with its finite element implementation can be found in Yin et al. [16,36]. To help identify the rate-dependent parameters, the initial void ratio, e_0, the swelling index, κ, and the compression index, λ, with the permeability (k=3.3×10^{-9} m/s) provided by Lee and Fahey [87] were fixed in the parameter identification. Note that the swelling index κ, the compression index λ and the permeability k could not be put into the Bayesian-based identification process since test results of oedometer tests and excess pore pressure measurements in SBP testing are not available. The Poisson's ratio υ was assumed to be 0.3 for soft clays [38]. The other parameters (the slope of critical state line M, the initial pre-consolidation pressure σ'_{p0}, and the secondary compression coefficient $C_{\alpha e}$) were determined by Bayesian identification with DE-TMCMC. The bounds of uniform distribution of parameters are given in Table 4. The settings of DE-TMCMC were same as those given previously. For purpose of comparison, the case was also carried out using O-TMCMC.

4.2 Results and discussions

Fig. 15 shows the posterior PDFs of three identified parameters of ANICREEP model using DE-TMCMC and O-TMCMC. The value of M distributes primarily in a large range within [1.5, 1.8] for DE-TMCMC, with an MAP value of 1.71, but for a narrow range [0.95, 1.05] for O-TMCMC, with an MAP value of 0.98. Similarly, the identified σ'_{p0} and $C_{\alpha e}$ also distribute in a large range for DE-TMCMC, with MAP values of 58.4 kPa and 0.020, compared to a narrow range for O-TMCMC, with MAP values of 102.6 kPa and 0.055. According to Low [88], it can be found that the identified M (=1.71) and σ'_{p0} (=58.4 kPa) were close to measured values and the identified parameter $C_{\alpha e}$=0.020 identical to the $C_{\alpha e}$=0.020 experimentally estimated by Low [88] based on the strain-rate dependency parameter β=0.055 of Burswood clay using the unified formulation of Yin et al. [89,90].

These comparisons demonstrate that much more reasonable parameters can be achieved through Bayesian parameter identification with DE-TMCMC than those with O-TMCMC.

All parameters of ANICREEP for Burswood clay are summarized in Table 5. Using all solutions obtained by DE-TMCMC, numerous simulations of two pressuremeter tests were performed. Fig. 16 compares the predictions with uncertainties and measurements for the SBP tests in terms of total pressure at the cavity wall versus cavity strain. The measurements are mostly covered by the simulations. Accordingly, all findings demonstrate that the Bayesian parameter identification using the DE-TMCMC is efficient and applicable for in-situ testing.

5 Discussions

Using statistical methods in calibrating has a long tradition in soil mechanics, which has been reviewed in the introduction. As the calibrating procedure is an inverse problem and the solution is generally not unique, i.e. many parameter combinations provide similar acceptable results in the sense that a user defined error measurement is small enough [41,14,42]. Moreover, the solutions depend on user defined error measurement, for which no general rule exists. However, the performance of error function in the likelihood defined in the proposed method has been highlighted in various cases [13,14,2,37,34,35,42,36,38]. The defined error function considers both the effect of quantities for different test curves (such as deviatoric stress-axial strain curve for different confining pressures) and the effect of dimension/unit for different variables (such as deviatoric stress and volumetric strain in same test). Thus, a set of reliable parameters totally reflecting the material behaviours can be obtained by the proposed method.

In traditional calibration, one uses experiments suitable for calibrating sub sets of the material parameters. The critical state friction angle, for example, can be calibrated from three triaxial tests, without considering other parameters like elastic stiffness. Although one gets a better feeling of the specific parameter influences a specific behaviour of the soil by doing such calibration works, such way can be successful only for few conventional laboratory tests, such as 1D compression and 3D triaxial tests. Identification of parameters from in-situ or field tests cannot be completed by such kind of traditional calibration methods. Moreover, the amount of parameters directly determined by such way is limited. With the development of constitutive modelling, numerous advanced soil models

with a large number of parameters have been proposed [36]. The traditional calibration method becomes ineffective for a large number of parameters, in particular becomes invalid for parameters without clear physical meaning. For this situation, the trial and error method is usually used. In practice, such calibrations often depend on the user's preferences and experiences. In that sense, calibrating of material parameters by the proposed method is more competitive than by traditional calibration methods.

Furthermore, the local convergence problem inevitably exists for most inverse methods. However, the proposed Bayesian identification with DE-TMCMC has the ability to prevent the identification process from the local convergence, which has been demonstrated by aforementioned results and the comparisons to original TMCMC (see Figs. 10 and 11).

Overall, the proposed Bayesian parameter identification has advantages in dealing with different parameter calibration works, even when some parameters have non-physical meaning.

6 Conclusions

To identify parameters also considering soil uncertainty, a method of Bayesian parameter identification using an enhanced DE-TMCMC with parallel computing technique has been developed in this paper. The DE-TMCMC, enhanced through implementing a differential evolution into TMCMC to replace the process of proposing a new sample, has been proposed. To save on computational costs, a parallel computing DE-TMCMC was achieved by implementing the SPMD technique.

The performance of DE-TMCMC during Bayesian parameter identification was first validated through comparison to the original TMCMC for the case of identifying parameters of a critical state–based model from triaxial tests in terms of robustness and effectiveness: three synthetic drained triaxial tests with/without noise for numerical validation, and three real drained triaxial tests on Toyoura sand for applicability. To avoid randomness, the calculations were independently conducted 10 times. The results demonstrate that the DE-TMCMC is highly robust and efficient, producing reasonably ranged posterior PDFs as well as a set of accurate parameters regardless of whether the used data is noisy.

Finally, the enhanced DE-TMCMC based parameter identification approach was applied to two in-situ pressuremeter tests on soft clays. The elastic viscoplastic model ANICREEP was adopted to take into account the time effect for clays. The identified MAP parameters agree well with values measured in oedometer and triaxial tests, indicating a high level of efficiency for the proposed approach and the applicability to the in-situ testing.

In addition to the parameter identification by DE-TMCMC, the approach can also be used to estimate the evidence of the chosen probabilistic model class conditioning on the measured data, a key component for Bayesian model class selection and model averaging [68,67]. Therefore, future works will focus on the application of this approach to Bayesian model class selection and model averaging in geotechnical engineering through use of advanced soil models.

Acknowledgments

The financial support for this research came from the National Natural Science Foundation of China (No. 51579179) and the Macau Science and Technology Development Fund (FDCT/125/2014/A3).

Appendix-introduction of SIMSAND

The selected critical state–based sand model was SIMSAND, which has seen widely used in various studies [13,2,37,91]. Accordingly, only basic principles were introduced herein for ease of understanding. Consistently with the elastoplastic theory, the total strain rate is composed of the elastic and plastic strain rates:

$$\delta\varepsilon_{ij} = \delta\varepsilon_{ij}^{el} + \delta\varepsilon_{ij}^{pl} \quad \text{(I)}$$

where $\delta\varepsilon_{ij}$ denotes the (*i*, *j*) the total strain rate tensor, and the superscripts *el* and *pl* represent the elastic and plastic components, respectively.

The nonlinear elastic behaviour is assumed to be isotropic with the Young's modulus *E*:

$$\delta\varepsilon_{ij}^{el} = \frac{1+\upsilon}{E}\delta\sigma'_{ij} - \frac{\upsilon}{E}\delta\sigma'_{kk}\delta_{ij} \quad \text{(II)}$$

where υ is Poisson's ratio, $\delta\sigma'_{ij}$ is the effective stress rate tensor, and δ_{ij} is the Kronecker's delta. *E* is calculated by using the isotropic elastic bulk modulus *K* by $E=3K(1-2\upsilon)$, and for sand, is defined as:

$$K = K_0 p_{at} \frac{(2.97-e)^2}{(1+e)} \left(\frac{p'}{p_{at}}\right)^n \quad \text{(III)}$$

where K_0 and *n* are elastic parameters, *e* is void ratio, p' is the mean effective stress, and p_{at} is the atmospheric pressure (p_{at} = 101.325 kPa).

The yield surface for shear sliding can be expressed as,

$$f = \frac{q}{p'} - \frac{M_p \varepsilon_d^p}{k_p + \varepsilon_d^p} = 0 \quad \text{(IV)}$$

where *q* is the deviatoric stress, k_p is related to the plastic shear modulus, M_p is stress ratio corresponding to the peak strength calculated by the peak friction angle ϕ_p ($M_p=6\sin(\phi_p)/(3-\sin(\phi_p))$ in compression), and ε_d^p is the deviatoric plastic strain.

The gradient of the plastic potential surface for stress-dilatancy *g* can be expressed as:

$$\frac{\partial g}{\partial \sigma_{ij}} = \frac{\partial g}{\partial p'}\frac{\partial p'}{\partial \sigma_{ij}} + \frac{\partial g}{\partial q}\frac{\partial q}{\partial \sigma_{ij}} \text{ with } \frac{\partial g}{\partial p'} = A_d\left(M_{pt} - \frac{q}{p'}\right);\ \frac{\partial g}{\partial q} = 1 \quad \text{(V)}$$

where A_d is the stress-dilatancy parameter, and M_{pt} can be calculated from the phase transformation friction angle ϕ_{pt} ($M_{pt}=6\sin(\phi_{pt})/(3-\sin(\phi_{pt}))$ in compression). The double index ij is simplified as $1 \hat{=} 11,\ 2 \hat{=} 22,\ 3 \hat{=} 33,\ 4 \hat{=} 12,\ 5 \hat{=} 23,\ 6 \hat{=} 31$.

A nonlinear critical state line (CSL) formulation to guarantee the positiveness of the critical void ratio was well suited to sand modelling,

$$e_c = e_{ref} \exp\left[-\lambda\left(\frac{p'}{p_{at}}\right)^{\xi}\right] \tag{VI}$$

where e_c is the critical void ratio, e_{ref} is the initial critical void ratio at $p' = 0$, and λ and ξ are the parameters controlling the shape of CSL in the e-logp' plane.

Soil density and the interlocking grains effects are introduced through the expression of the friction angle as:

$$\tan\phi_p = \left(\frac{e_c}{e}\right)^{n_p} \tan\phi_u; \quad \tan\phi_{pt} = \left(\frac{e_c}{e}\right)^{-n_d} \tan\phi_\mu \tag{VII}$$

where the parameters n_p and n_d are material constants, and ϕ_μ is friction angle at critical state. The Lode angle dependent strength and stress-dilatancy are introduced as described in Sheng et al. [92], but could also be incorporated by using the transformed stress method of Yao et al. [93,8,94,9].

All parameters of the sand model can be divided into three groups: (1) elasticity parameters (K_0, υ and n), (2) *CSL*-related parameters (e_{ref}, λ, ξ and ϕ_μ), and (3) interlocking-related parameters (A_d, k_p, n_p and n_d).

References

1. Vermeer P (1978) A double hardening model for sand. Geotechnique 28 (4):413-433
2. Jin Y-F, Yin Z-Y, Shen S-L, Hicher P-Y (2016) Selection of sand models and identification of parameters using an enhanced genetic algorithm. Int J Numer Anal Methods Geomech 40 (8):1219-1240. doi:10.1002/nag.2487
3. Kolymbas D (1991) An outline of hypoplasticity. Archive of applied mechanics 61 (3):143-151
4. Roscoe KH, Burland J (1968) On the generalized stress-strain behaviour of wet clay. Paper presented at the Engineering Plasticity, Cambridge, UK,
5. Jefferies M (1993) Nor-Sand: a simle critical state model for sand. Geotechnique 43 (1):91-103
6. Yu H (1998) CASM: A unified state parameter model for clay and sand. Int J Numer Anal Methods Geomech 22 (8):621-653
7. Gajo A, Wood M (1999) Severn–Trent sand: a kinematic-hardening constitutive model: the q–p formulation. Geotechnique 49 (5):595-614
8. Yao Y, Hou W, Zhou A (2009) UH model: three-dimensional unified hardening model for overconsolidated clays. Geotechnique 59 (5):451-469
9. Yao Y, Sun D, Luo T (2004) A critical state model for sands dependent on stress and density. Int J Numer Anal Methods Geomech 28 (4):323-337
10. Yao Y, Sun D, Matsuoka H (2008) A unified constitutive model for both clay and sand with hardening parameter independent on stress path. Computers and Geotechnics 35 (2):210-222
11. Yao Y-P, Kong L-M, Zhou A-N, Yin J-H (2014) Time-dependent unified hardening model: Three-dimensional elastoviscoplastic constitutive model for clays. Journal of engineering mechanics 141 (6):04014162
12. Taiebat M, Dafalias YF (2008) SANISAND: Simple anisotropic sand plasticity model. Int J Numer Anal Methods Geomech 32 (8):915-948
13. Jin Y-F, Wu Z-X, Yin Z-Y, Shen JS (2017) Estimation of critical state-related formula in advanced constitutive modeling of granular material. Acta Geotech 12 (6):1329-1351. doi:10.1007/s11440-017-0586-5
14. Jin Y-F, Yin Z-Y, Shen S-L, Hicher P-Y (2016) Investigation into MOGA for identifying parameters of a critical-state-based sand model and parameters correlation by factor analysis. Acta Geotech 11 (5):1131-1145. doi:10.1007/s11440-015-0425-5
15. Yin ZY, Chang CS, Karstunen M, Hicher PY (2010) An anisotropic elastic-viscoplastic model for soft clays. Int J Solids Struct 47 (5):665-677
16. Yin ZY, Karstunen M, Chang CS, Koskinen M, Lojander M (2011) Modeling Time-Dependent Behavior of Soft Sensitive Clay. Journal of geotechnical and geoenvironmental engineering 137 (11):1103-1113. doi:10.1061/(asce)gt.1943-5606.0000527
17. Mašín D (2005) A hypoplastic constitutive model for clays. Int J Numer Anal Methods Geomech 29 (4):311-336
18. Wu W, Bauer E, Kolymbas D (1996) Hypoplastic constitutive model with critical state for granular materials. Mech Mater 23 (1):45-69

19. Wang S, Wu W, Yin Z-Y, Peng C, He X-Z (2018) Modelling time-dependent behaviour of granular material with hypoplasticity. Int J Numer Anal Methods Geomech 42 (12):1331-1345. doi:https://doi.org/10.1002/nag.2793
20. Von Wolffersdorff PA (1996) A hypoplastic relation for granular materials with a predefined limit state surface. Mechanics of Cohesive‐frictional Materials: An International Journal on Experiments, Modelling and Computation of Materials and Structures 1 (3):251-271
21. Kolymbas D (1985) A generalized hypoelastic constitutive law. Paper presented at the Proc. XI Int. Conf. Soil Mechanics and Foundation Engineering, San Francisco,
22. Chang CS, Hicher PY (2005) An elasto-plastic model for granular materials with microstructural consideration. Int J Solids Struct 42 (14):4258-4277. doi:http://dx.doi.org/10.1016/j.ijsolstr.2004.09.021
23. Yin ZY, Chang CS, Hicher PY, Karstunen M (2009) Micromechanical analysis of kinematic hardening in natural clay. Int J Plast 25 (8):1413-1435
24. Yin ZY, Chang CS, Hicher PY (2010) Micromechanical modelling for effect of inherent anisotropy on cyclic behaviour of sand. Int J Solids Struct 47 (14-15):1933-1951. doi:10.1016/j.ijsolstr.2010.03.028
25. Yin Z-Y, Zhao J, Hicher P-Y (2014) A micromechanics-based model for sand-silt mixtures. Int J Solids Struct 51 (6):1350-1363
26. Yin Z, Chang C, Hicher P, Karstunen M (2008) Microstructural Modeling of Rate-dependent Behavior of Soft Soil.
27. Yin ZY, Chang CS (2009) Microstructural modelling of stress-dependent behaviour of clay. Int J Solids Struct 46 (6):1373-1388
28. Xiong H, Nicot F, Yin Z (2017) A three‐dimensional micromechanically based model. Int J Numer Anal Methods Geomech 41 (17):1669-1686
29. Shen SL, Xu YS (2011) Numerical evaluation of land subsidence induced by groundwater pumping in Shanghai. Canadian Geotechnical Journal 48 (9):1378-1392
30. Wu H-N, Shen S-L, Yang J (2017) Identification of tunnel settlement caused by land subsidence in soft deposit of Shanghai. Journal of Performance of Constructed Facilities 31 (6):04017092
31. Xu Y-S, Ma L, Shen S-L, Sun W-J (2012) Evaluation of land subsidence by considering underground structures that penetrate the aquifers of Shanghai, China. Hydrol J 20 (8):1623-1634
32. Shen S-L, Wu Y-X, Misra A (2017) Calculation of head difference at two sides of a cut-off barrier during excavation dewatering. Computers and Geotechnics 91:192-202
33. Ren D-J, Shen S-L, Arulrajah A, Wu H-N (2018) Evaluation of ground loss ratio with moving trajectories induced in DOT tunnelling. Canadian Geotechnical Journal 55 (6):894-902
34. Jin Y-F, Yin Z-Y, Wu Z-X, Daouadji A (2018) Numerical modeling of pile penetration in silica sands considering the effect of grain breakage. Finite Elem Anal Des 144:15-29. doi:https://doi.org/10.1016/j.finel.2018.02.003
35. Jin Y-F, Yin Z-Y, Wu Z-X, Zhou W-H (2018) Identifying parameters of easily crushable sand and application to offshore pile driving. Ocean Eng 154:416-429. doi:10.1016/j.oceaneng.2018.01.023

36. Yin Z-Y, Jin Y-F, Shen JS, Hicher P-Y (2018) Optimization techniques for identifying soil parameters in geotechnical engineering: Comparative study and enhancement. Int J Numer Anal Methods Geomech 42 (1):70-94. doi:10.1002/nag.2714
37. Jin Y-F, Yin Z-Y, Shen S-L, Zhang D-M (2017) A new hybrid real-coded genetic algorithm and its application to parameters identification of soils. Inverse Problems in Science and Engineering 25 (9):1343-1366. doi:10.1080/17415977.2016.1259315
38. Yin Z-Y, Jin Y-F, Shen S-L, Huang H-W (2017) An efficient optimization method for identifying parameters of soft structured clay by an enhanced genetic algorithm and elastic–viscoplastic model. Acta Geotech 12 (4):849-867. doi:10.1007/s11440-016-0486-0
39. Knabe T, Datcheva M, Lahmer T, Cotecchia F, Schanz T (2013) Identification of constitutive parameters of soil using an optimization strategy and statistical analysis. Computers and Geotechnics 49:143-157. doi:10.1016/j.compgeo.2012.10.002
40. Levasseur S, Malécot Y, Boulon M, Flavigny E (2008) Soil parameter identification using a genetic algorithm. Int J Numer Anal Methods Geomech 32 (2):189-213. doi:10.1002/nag.614
41. Papon A, Riou Y, Dano C, Hicher PY (2012) Single-and multi-objective genetic algorithm optimization for identifying soil parameters. Int J Numer Anal Methods Geomech 36 (5):597-618. doi:10.1002/nag.1019
42. Jin Y-F, Yin Z-Y, Zhou W-H, Huang H-W (2019) Multi-objective optimization-based updating of predictions during excavation. Eng Appl Artif Intell 78:102-123. doi:https://doi.org/10.1016/j.engappai.2018.11.002
43. Zhang X, Srinivasan R, Bosch D (2009) Calibration and uncertainty analysis of the SWAT model using Genetic Algorithms and Bayesian Model Averaging. J Hydrol 374 (3):307-317
44. Cao Z, Wang Y (2014) Bayesian model comparison and selection of spatial correlation functions for soil parameters. Structural Safety 49:10-17
45. Miro S, König M, Hartmann D, Schanz T (2015) A probabilistic analysis of subsoil parameters uncertainty impacts on tunnel-induced ground movements with a back-analysis study. Computers and Geotechnics 68:38-53
46. Ritto T, Nunes L (2015) Bayesian model selection of hyperelastic models for simple and pure shear at large deformations. Computers & Structures 156:101-109
47. Akeju OV, Senetakis K, Wang Y (2017) Bayesian parameter identification and model selection for normalized modulus reduction curves of soils. J Earthquake Eng 1-29
48. Zhang L, Li D-Q, Tang X-S, Cao Z-J, Phoon K-K (2017) Bayesian model comparison and characterization of bivariate distribution for shear strength parameters of soil. Computers and Geotechnics 95:110-118
49. Cividini A, Maier G, Nappi A Parameter estimation of a static geotechnical model using a Bayes' approach. In: International Journal of Rock Mechanics and Mining Sciences & Geomechanics Abstracts, 1983. Elsevier, pp 215-226
50. Murakami A, Shinmura H, Ohno S, Fujisawa K (2017) Model identification and parameter estimation of elastoplastic constitutive model by data assimilation using the particle filter. Int J Numer Anal Methods Geomech

51. Hsiao EC, Schuster M, Juang CH, Kung GT (2008) Reliability Analysis and Updating of Excavation-Induced Ground Settlement for Building Serviceability Assessment. Journal of Geotechnical & Geoenvironmental Engineering 134 (10):1448-1458
52. Juang C, Hsein , Luo Z, Atamturktur S, Huang H (2012) Bayesian updating of soil parameters for braced excavations using field observations. Journal of geotechnical and geoenvironmental engineering 139 (3):395-406
53. Most T (2010) Identification of the parameters of complex constitutive models: Least squares minimization vs. Bayesian updating. Reliability and Optimization of Structural Systems 119
54. Honjo Y, Wen‐Tsung L, Guha S (1994) Inverse analysis of an embankment on soft clay by extended Bayesian method. Int J Numer Anal Methods Geomech 18 (10):709-734
55. Qi X-H, Zhou W-H (2017) An efficient probabilistic back-analysis method for braced excavations using wall deflection data at multiple points. Computers and Geotechnics 85:186-198
56. Ancey C (2005) Monte Carlo calibration of avalanches described as Coulomb fluid flows. Philosophical Transactions of the Royal Society A: Mathematical, Physical and Engineering Sciences 363 (1832):1529-1550
57. Eckert N, Parent E, Richard D (2007) Revisiting statistical–topographical methods for avalanche predetermination: Bayesian modelling for runout distance predictive distribution. Cold Reg Sci Technol 49 (1):88-107
58. Fischer J-T, Kofler A, Fellin W, Granig M, Kleemayr K (2015) Multivariate parameter optimization for computational snow avalanche simulation. Journal of Glaciology 61 (229):875-888
59. Gauer P, Medina-Cetina Z, Lied K, Kristensen K (2009) Optimization and probabilistic calibration of avalanche block models. Cold Reg Sci Technol 59 (2-3):251-258
60. Hellweger V, Fischer J-T, Kofler A, Huber A, Fellin W, Oberguggenberger M (2016) Stochastic Methods in Operational Avalanche Simulation - From Back Calculation to Prediction. Paper presented at the International Snow Science Workshop 2016 Proceedings, Colorado, USA,
61. Tan F, Zhou WH, Yuen KV (2018) Effect of loading duration on uncertainty in creep analysis of clay. Int J Numer Anal Methods Geomech 42 (11):1235-1254
62. Zhou W-H, Tan F, Yuen K-V (2018) Model updating and uncertainty analysis for creep behavior of soft soil. Computers and Geotechnics 100:135-143. doi:https://doi.org/10.1016/j.compgeo.2018.04.006
63. Zhang J, Zhang LM, Tang WH (2009) Bayesian Framework for Characterizing Geotechnical Model Uncertainty. Journal of Geotechnical and Geoenvironmental Engineering 135 (7):932-940. doi:doi:10.1061/(ASCE)GT.1943-5606.0000018
64. Zhang R, Mahadevan S (2000) Model uncertainty and Bayesian updating in reliability-based inspection. Structural Safety 22 (2):145-160
65. Zhang L, Zuo Z, Ye G, Jeng D, Wang J (2013) Probabilistic parameter estimation and predictive uncertainty based on field measurements for unsaturated soil slope. Computers and Geotechnics 48:72-81
66. Hastings WK (1970) Monte Carlo sampling methods using Markov chains and their applications. Biometrika 57 (1):97-109

67. Lee S-H, Song J (2017) System Identification of Spatial Distribution of Structural Parameters Using Modified Transitional Markov Chain Monte Carlo Method. Journal of engineering mechanics 143 (9):04017099
68. Ching J, Chen Y-C (2007) Transitional Markov chain Monte Carlo method for Bayesian model updating, model class selection, and model averaging. Journal of engineering mechanics 133 (7):816-832
69. Angelikopoulos P, Papadimitriou C, Koumoutsakos P (2015) X-TMCMC: Adaptive kriging for Bayesian inverse modeling. Computer Methods in Applied Mechanics and Engineering 289:409-428
70. Ortiz GA, Alvarez DA, Bedoya-Ruíz D (2015) Identification of Bouc–Wen type models using the transitional Markov chain Monte Carlo method. Computers & Structures 146:252-269
71. Betz W, Papaioannou I, Straub D (2016) Transitional markov chain monte carlo: observations and improvements. Journal of engineering mechanics 142 (5):04016016
72. Ching J, Wang J-S (2016) Application of the transitional Markov chain Monte Carlo algorithm to probabilistic site characterization. Eng Geol 203:151-167
73. Yuen K-V (2010) Bayesian methods for structural dynamics and civil engineering. John Wiley & Sons,
74. Beck JL (2010) Bayesian system identification based on probability logic. Structural Control and Health Monitoring 17 (7):825-847
75. Beck JL, Katafygiotis LS (1998) Updating models and their uncertainties. I: Bayesian statistical framework. Journal of engineering mechanics 124 (4):455-461
76. Yuen K-V (2010) Recent developments of Bayesian model class selection and applications in civil engineering. Structural Safety 32 (5):338-346
77. Yuen KV, Mu HQ (2015) Real‐time system identification: an algorithm for simultaneous model class selection and parametric identification. Computer‐Aided Civil and Infrastructure Engineering 30 (10):785-801
78. Tan F, Zhou W-H, Yuen K-V (2016) Modeling the soil water retention properties of same-textured soils with different initial void ratios. J Hydrol 542:731-743
79. He J, Jones JW, Graham WD, Dukes MD (2010) Influence of likelihood function choice for estimating crop model parameters using the generalized likelihood uncertainty estimation method. Agricultural Systems 103 (5):256-264
80. Chopin N (2002) A sequential particle filter method for static models. Biometrika 89 (3):539-552
81. Vrugt JA (2016) Markov chain Monte Carlo simulation using the DREAM software package: Theory, concepts, and MATLAB implementation. Environmental Modelling & Software 75:273-316
82. Angelikopoulos P, Papadimitriou C, Koumoutsakos P (2012) Bayesian uncertainty quantification and propagation in molecular dynamics simulations: a high performance computing framework. The Journal of chemical physics 137 (14):144103
83. Hadjidoukas PE, Angelikopoulos P, Papadimitriou C, Koumoutsakos P (2015) Π4U: A high performance computing framework for Bayesian uncertainty quantification of complex models. J Comput Phys 284:1-21

84. Verdugo R, Ishihara K (1996) The steady state of sandy soils. Soils and Foundations 36 (2):81-91
85. Wu Z-X, Yin Z-Y, Jin Y-F, Geng X-Y (2017) A straightforward procedure of parameters determination for sand: a bridge from critical state based constitutive modelling to finite element analysis. European Journal of Environmental and Civil Engineering:1-23. doi:10.1080/19648189.2017.1353442
86. Mašín D (2015) The influence of experimental and sampling uncertainties on the probability of unsatisfactory performance in geotechnical applications. Géotechnique 65 (11):897-910
87. Lee Goh A, Fahey M Application of a 1-dimensional cavity expansion model to pressuremeter and piezocone tests in clay. In: Proceeding of the Seventh International Conference on Computer Methods and Advances in Geomechanics, Cairns, 1991. pp 255-260
88. Low HE (2009) Performance of penetrometers in deepwater soft soil characterisation. University of Western Australia,
89. Yin Z-Y, Zhu Q-Y, Yin J-H, Ni Q (2014) Stress relaxation coefficient and formulation for soft soils. Géotechnique Letters 4 (January-March):45-51
90. Yin Z-Y, Yin J-H, Huang H-W (2015) Rate-Dependent and Long-Term Yield Stress and Strength of Soft Wenzhou Marine Clay: Experiments and Modeling. Marine Georesources & Geotechnology 33 (1):79-91
91. Wu Z-X, Yin Z-Y, Jin Y-F, Geng X-Y (2017) A straightforward procedure of parameters determination for sand: a bridge from critical state based constitutive modelling to finite element analysis. European Journal of Environmental and Civil Engineering:In press
92. Sheng D, Sloan S, Yu H (2000) Aspects of finite element implementation of critical state models. Comput Mech 26 (2):185-196
93. Yao Y-P, Wang N-D (2013) Transformed stress method for generalizing soil constitutive models. Journal of Engineering Mechanics 140 (3):614-629
94. Yao Y, Lu D, Zhou A, Zou B (2004) Generalized non-linear strength theory and transformed stress space. Sci China Ser E: Technol Sci 47 (6):691-709

Tables

Table 1 Identification results of SIMSAND from synthetic data and the bounds used in the calculation

Parameters	υ	K_0	n	e_{ref}	λ	ξ	ϕ_μ	k_p	A_d	n_p	n_d
Upper bound	-	-	-	1.5	0.1	1.0	50	0.01	2.0	0.1	0.1
Lower bound				0.5	0.001	0.01	20	0.0001	0.5	10.0	10.0
True value	0.2	100	0.6	0.750	0.03	0.60	30.0	0.003	1.0	2.0	2.0
Average $\boldsymbol{\theta}_{MAP}$ (without noise)				0.750	0.03	0.60	30.0	0.003	1.0	2.0	2.0
Average $\boldsymbol{\theta}_{MAP}$ (with noise)				0.753	0.034	0.57	30.05	0.0031	0.98	2.04	2.15

Table 2 Summary of triaxial tests on Toyoura sand

Test type	Drained tests						Undrained tests							
Test number	1	2	3	4	5	6	7	8	9	10	11	12	13	14
e_0	0.996	0.916	0.831	0.959	0.885	0.809	0.735				0.833			
p' / MPa	0.1	0.1	0.1	0.5	0.5	0.5	0.1	1	2	3	0.1	1	2	3

Table 3 Bounds in prior PDF, reference values, mean MAP values and standard deviations in posterior PDF for all parameters

Parameters	K_0	n	e_{ref}	λ	ξ	ϕ	k_p	A_d	n_p	n_d	σ_ε
and bounds	[50, 300]	[0.1, 0.9]	[0.5, 1.5]	[10^{-3}, 10^{-1}]	[0.1, 1.0]	[20, 50]	[10^{-3}, 10^{-1}]	[0.1, 2]	[0, 10]	[0, 10]	[0, 1]
$\boldsymbol{\theta}_{MAP}$ O-TMCMC	172.6 (13.2)	0.449 (0.029)	0.928 (0.004)	0.0212 (0.0016)	0.81 (0.028)	30.74 (0.67)	0.0010 (0.001)	0.68 (0.065)	5.35 (0.98)	5.00 (0.49)	0.28 (0.008)
$\boldsymbol{\theta}_{MAP}$ DE-TMCMC	144.6 (6.96)	0.463 (0.018)	0.904 (0.002)	0.0097 (6.62e-4)	0.933 (0.019)	32.18 (0.26)	0.0043 (4.42e-4)	0.42 (0.023)	3.157 (0.52)	4.24 (0.43)	0.057 (0.0055)
Reference values	130	0.5	0.920	0.0131	0.78	32.40	0.0030	0.50	1.60	4.10	-

Table 4 Search domain for three parameters of ANICREEP model

Parameters	M	σ'_{p0} / kPa	$C_{\alpha e}$
Lower bound	0.5	10	0.001
Upper bound	2.0	200	0.05

Table 5 MAP values of ANICREEP model for Burswood clay

MAP Parameters	υ	e_0	κ	λ	M	σ'_{p0} / kPa	$C_{\alpha e}$
DE-TMCMC	0.3	2.8	0.036	0.40	1.71	58.4	0.020
O-TMCMC					0.98	102.6	0.055

Figure captions

Figure 1

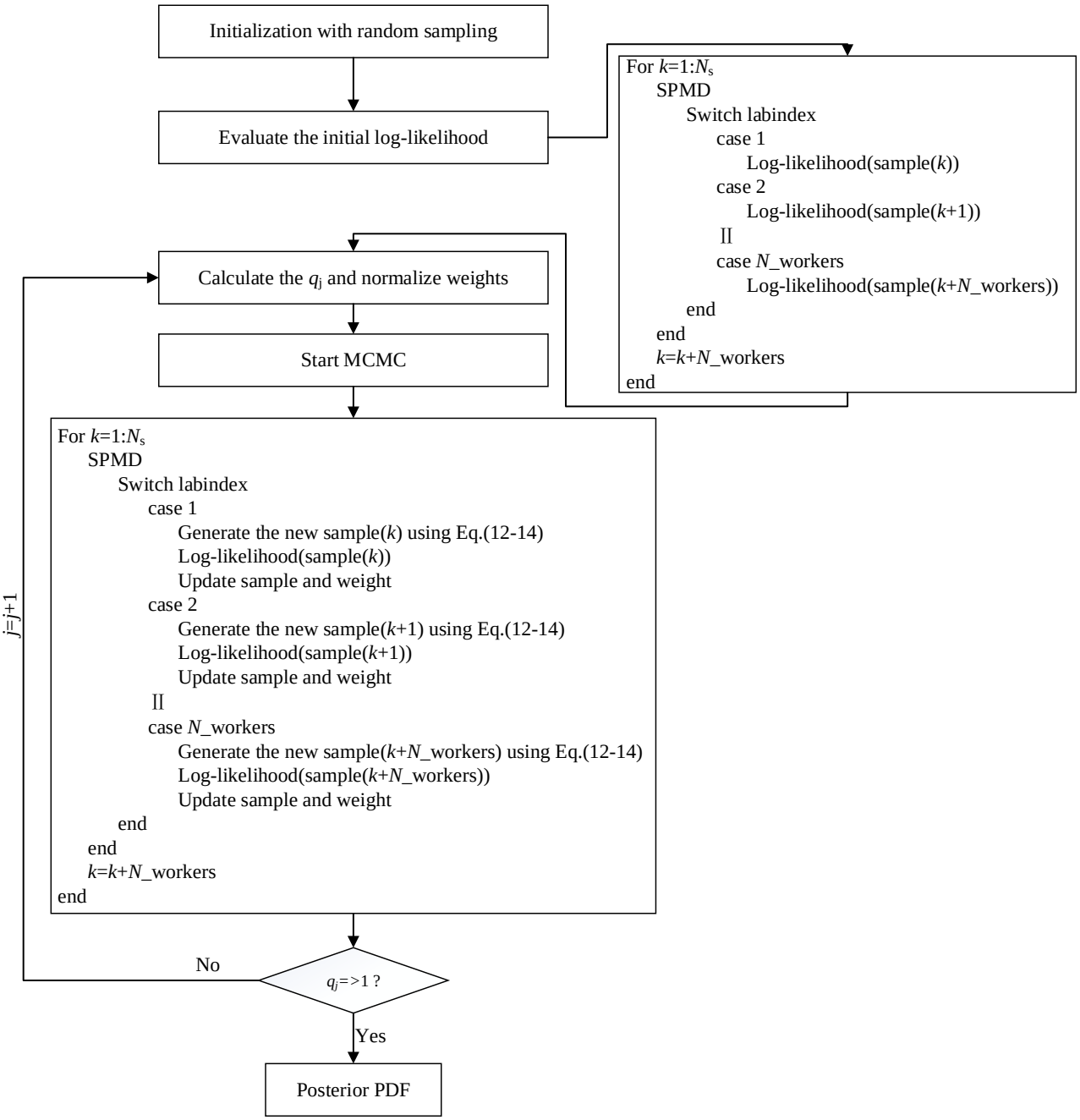
Initialization with random sampling
Evaluate the initial log-likelihood
For k=1:N_s
SPMD
Switch labindex
case 1
Log-likelihood(sample(k))
case 2
Log-likelihood(sample(k+1))
||
case N_workers
Log-likelihood(sample(k+N_workers))
end
end
k=k+N_workers
end
Calculate the q_j and normalize weights
Start MCMC
For k=1:N_s
SPMD
Switch labindex
case 1
Generate the new sample(k) using Eq.(12-14)
Log-likelihood(sample(k))
Update sample and weight
case 2
Generate the new sample(k+1) using Eq.(12-14)
Log-likelihood(sample(k+1))
Update sample and weight
||
case N_workers
Generate the new sample(k+N_workers) using Eq.(12-14)
Log-likelihood(sample(k+N_workers))
Update sample and weight
end
end
k=k+N_workers
end
j=j+1
No
q_j=>1 ?
Yes
Posterior PDF

Figure 2

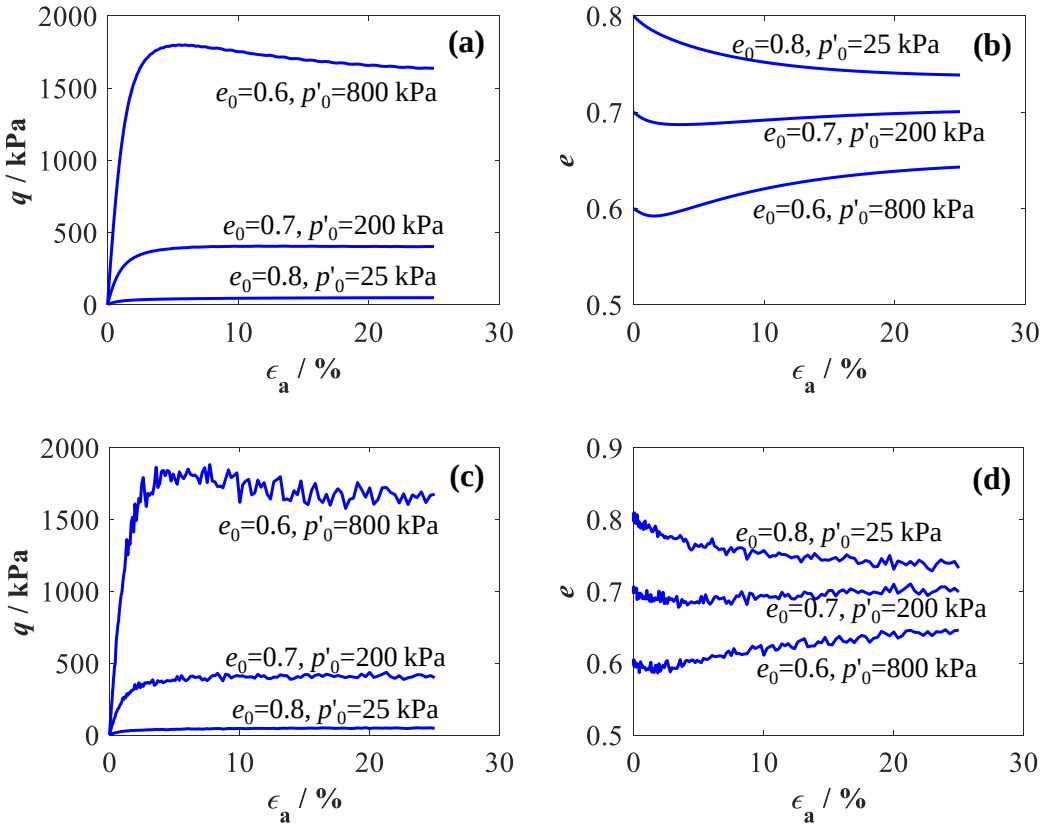
(a)
q / kPa
2000
1500
1000
500
0
0
10
20
30
ϵa / %
e0=0.6, p'0=800 kPa
e0=0.7, p'0=200 kPa
e0=0.8, p'0=25 kPa
(b)
e
0.8
0.7
0.6
0.5
e0=0.8, p'0=25 kPa
e0=0.7, p'0=200 kPa
e0=0.6, p'0=800 kPa
(c)
(d)
0.9

Figure 3

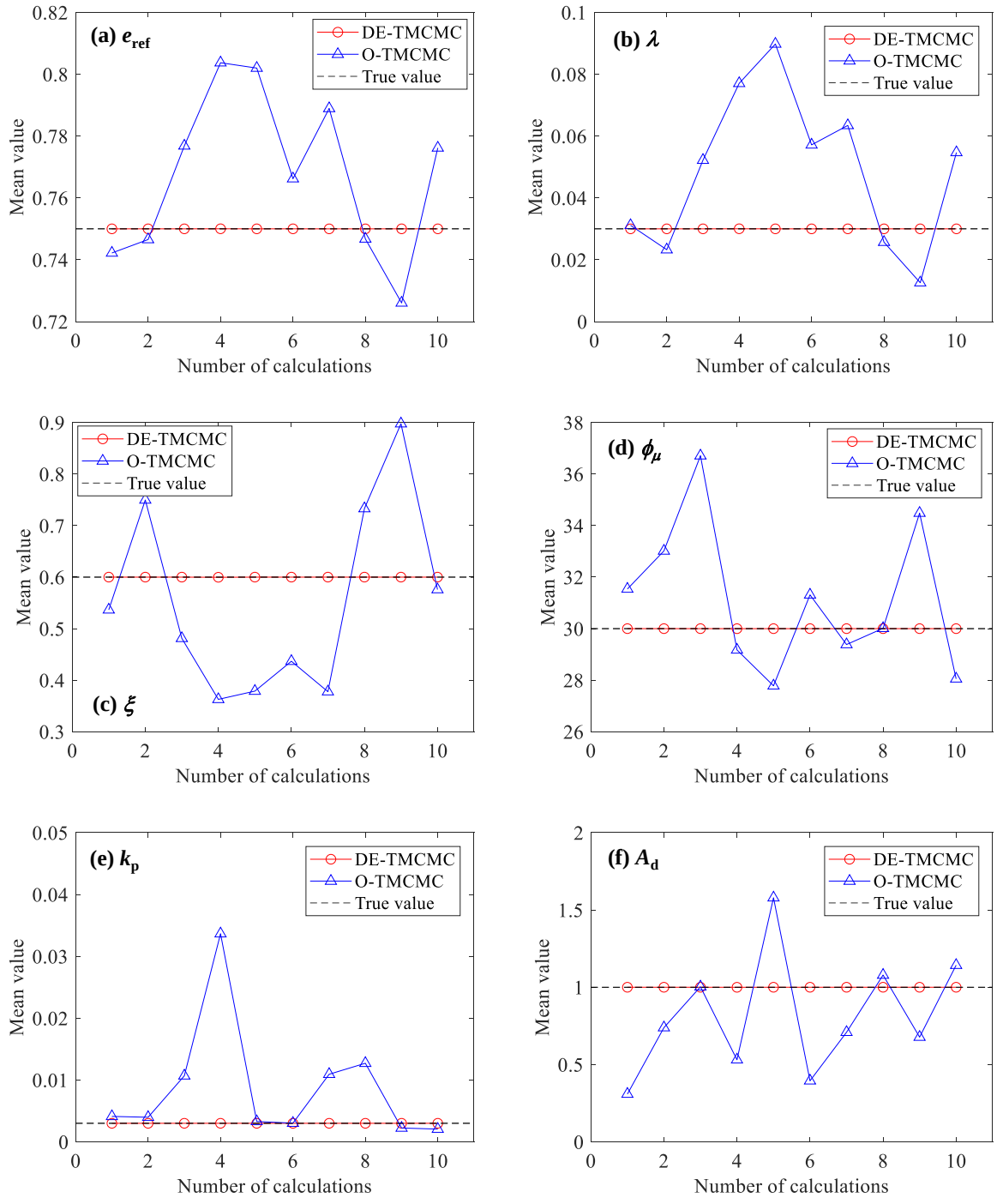
(a) e_{ref}
DE-TMCMC
O-TMCMC
True value
Mean value
Number of calculations
(b) λ
(c) ξ
(d) ϕ_μ
(e) k_p
(f) A_d

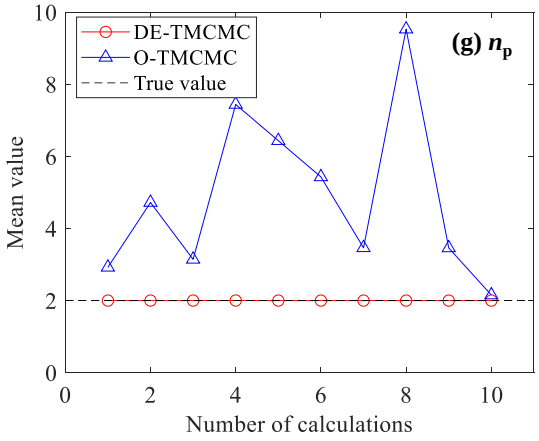
DE-TMCMC
O-TMCMC
True value
(g) n_p
Mean value
Number of calculations
0
2
4
6
8
10

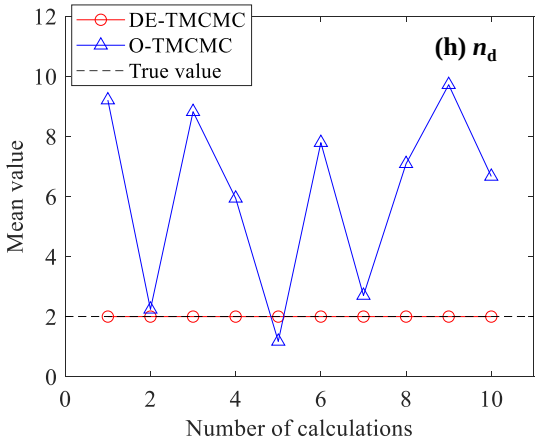
DE-TMCMC
O-TMCMC
True value
(h) n_d
Mean value
Number of calculations
0
2
4
6
8
10
12

Figure 4

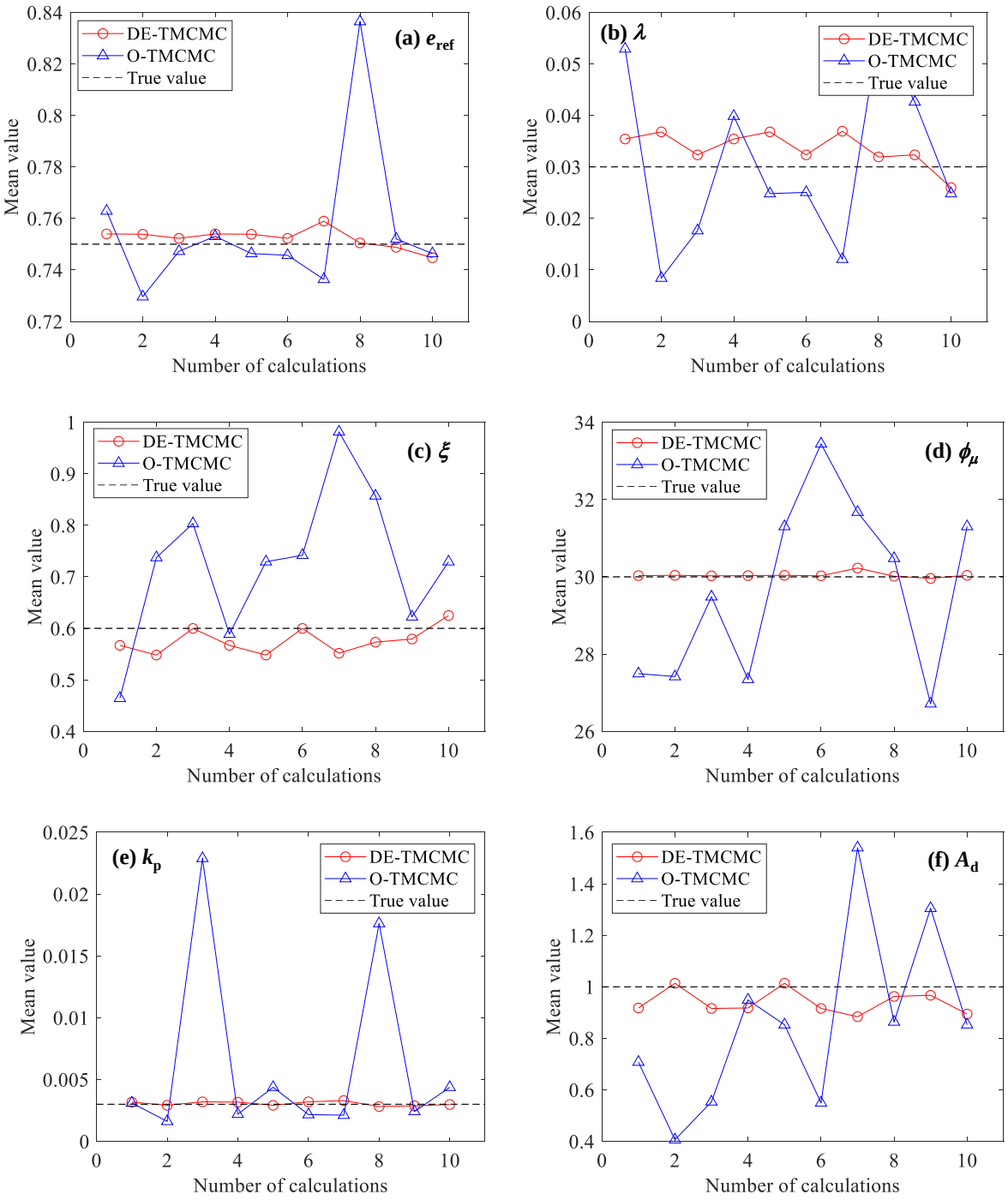
(a) e_{ref}
DE-TMCMC
O-TMCMC
True value
Mean value
Number of calculations
(b) λ
(c) ξ
(d) ϕ_μ
(e) k_p
(f) A_d

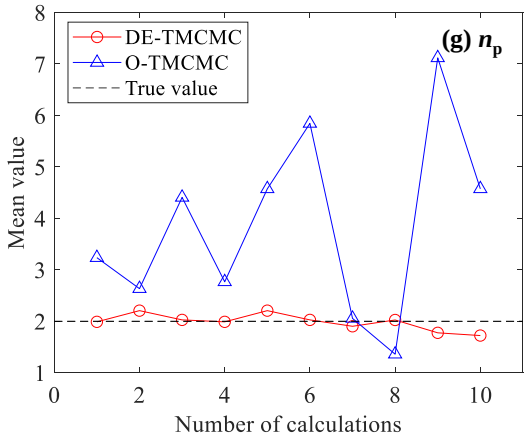
DE-TMCMC
O-TMCMC
True value
(g) n_p
Mean value
Number of calculations

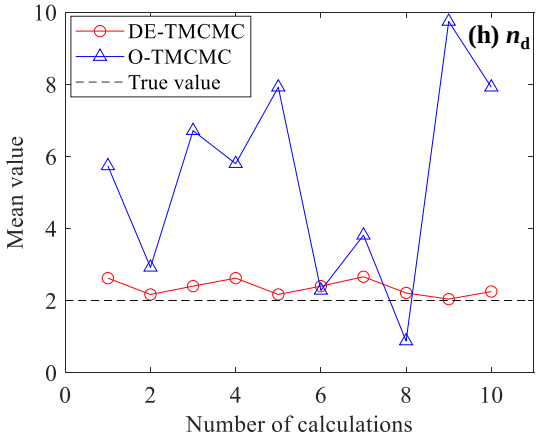
DE-TMCMC
O-TMCMC
True value
(h) n_d
Mean value
Number of calculations

Figure 5

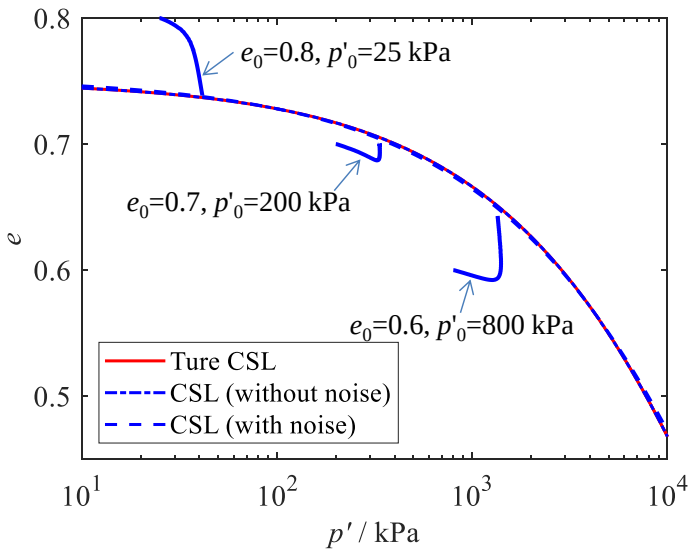
0.8
0.7
0.6
0.5
e
e_0=0.8, p'_0=25 kPa
e_0=0.7, p'_0=200 kPa
e_0=0.6, p'_0=800 kPa
Ture CSL
CSL (without noise)
CSL (with noise)
10^1
10^2
10^3
10^4
p' / kPa

Figure 6

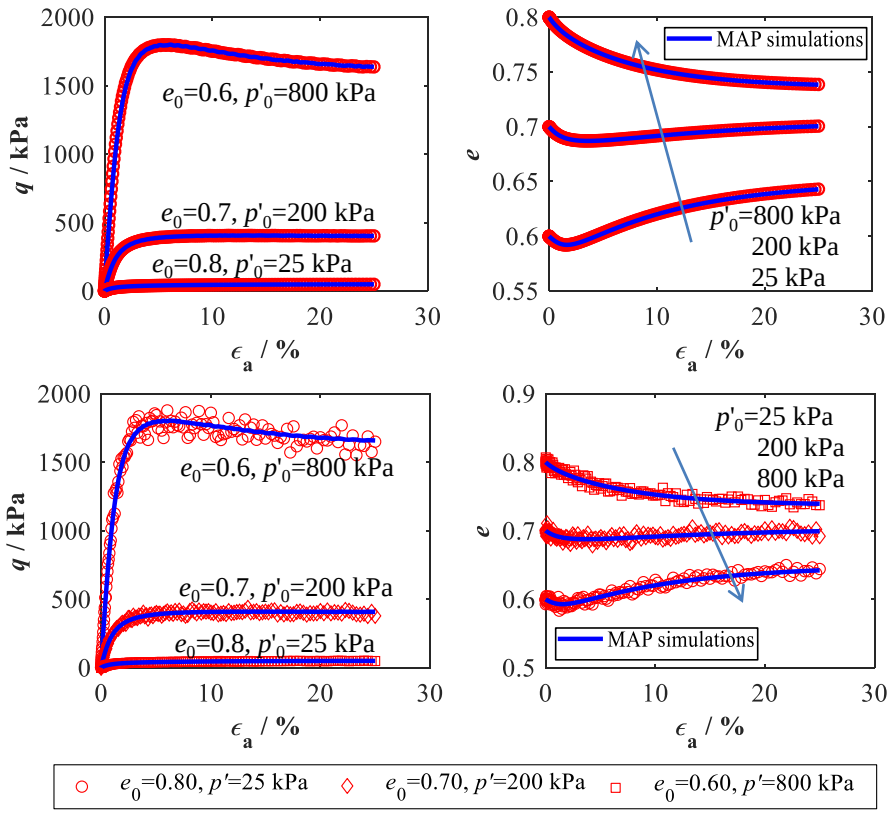
q / kPa
ϵa / %
e0=0.6, p'0=800 kPa
e0=0.7, p'0=200 kPa
e0=0.8, p'0=25 kPa
e
MAP simulations
p'0=800 kPa
200 kPa
25 kPa
p'0=25 kPa
200 kPa
800 kPa
e0=0.80, p'=25 kPa
e0=0.70, p'=200 kPa
e0=0.60, p'=800 kPa

Figure 7

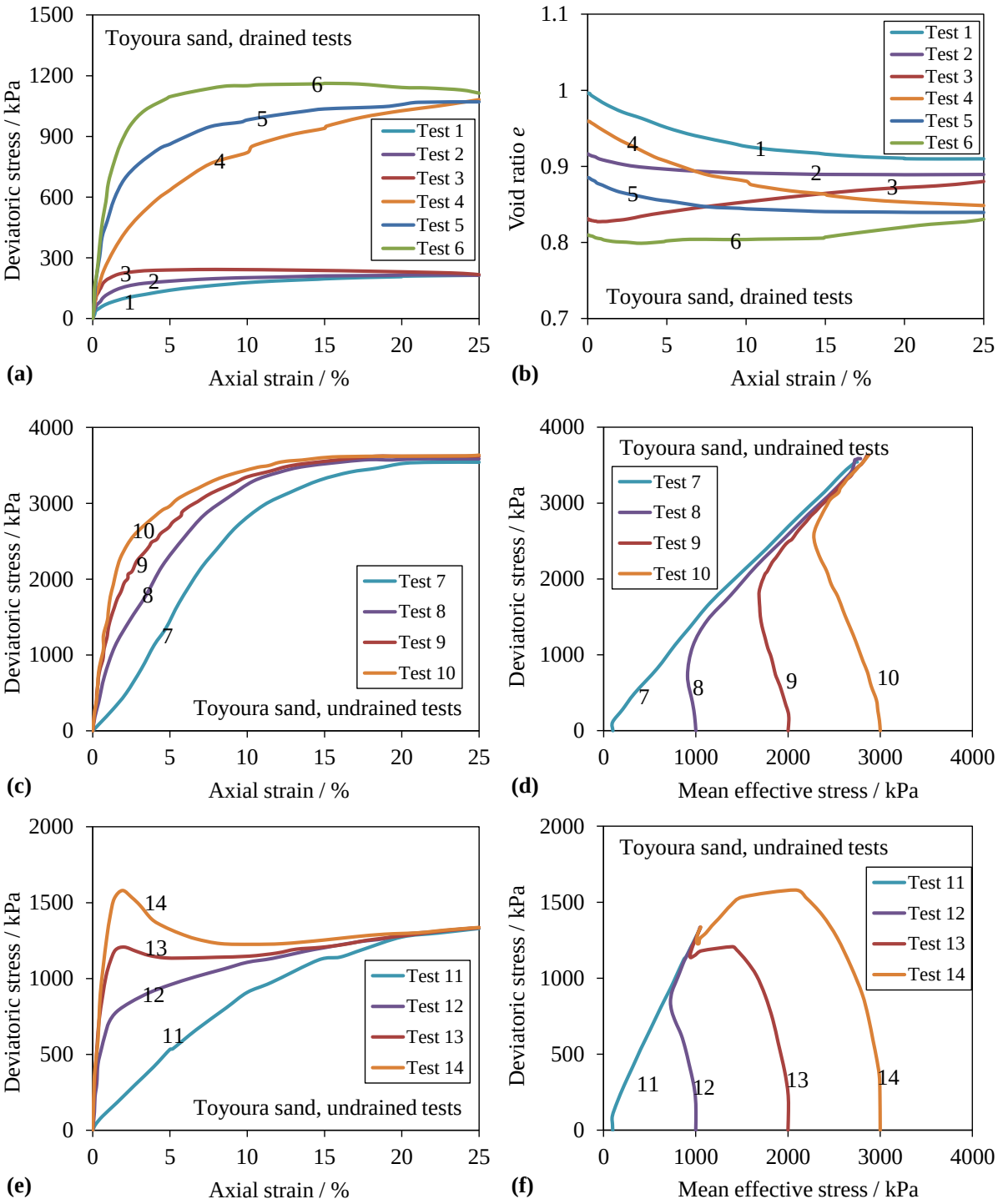
Toyoura sand, drained tests
Deviatoric stress / kPa
Axial strain / %
Test 1
Test 2
Test 3
Test 4
Test 5
Test 6
(a)
Void ratio e
Toyoura sand, drained tests
Axial strain / %
(b)
Toyoura sand, undrained tests
Deviatoric stress / kPa
Axial strain / %
Test 7
Test 8
Test 9
Test 10
(c)
Toyoura sand, undrained tests
Deviatoric stress / kPa
Mean effective stress / kPa
(d)
Toyoura sand, undrained tests
Deviatoric stress / kPa
Axial strain / %
Test 11
Test 12
Test 13
Test 14
(e)
Toyoura sand, undrained tests
Deviatoric stress / kPa
Mean effective stress / kPa
(f)

Figure 8

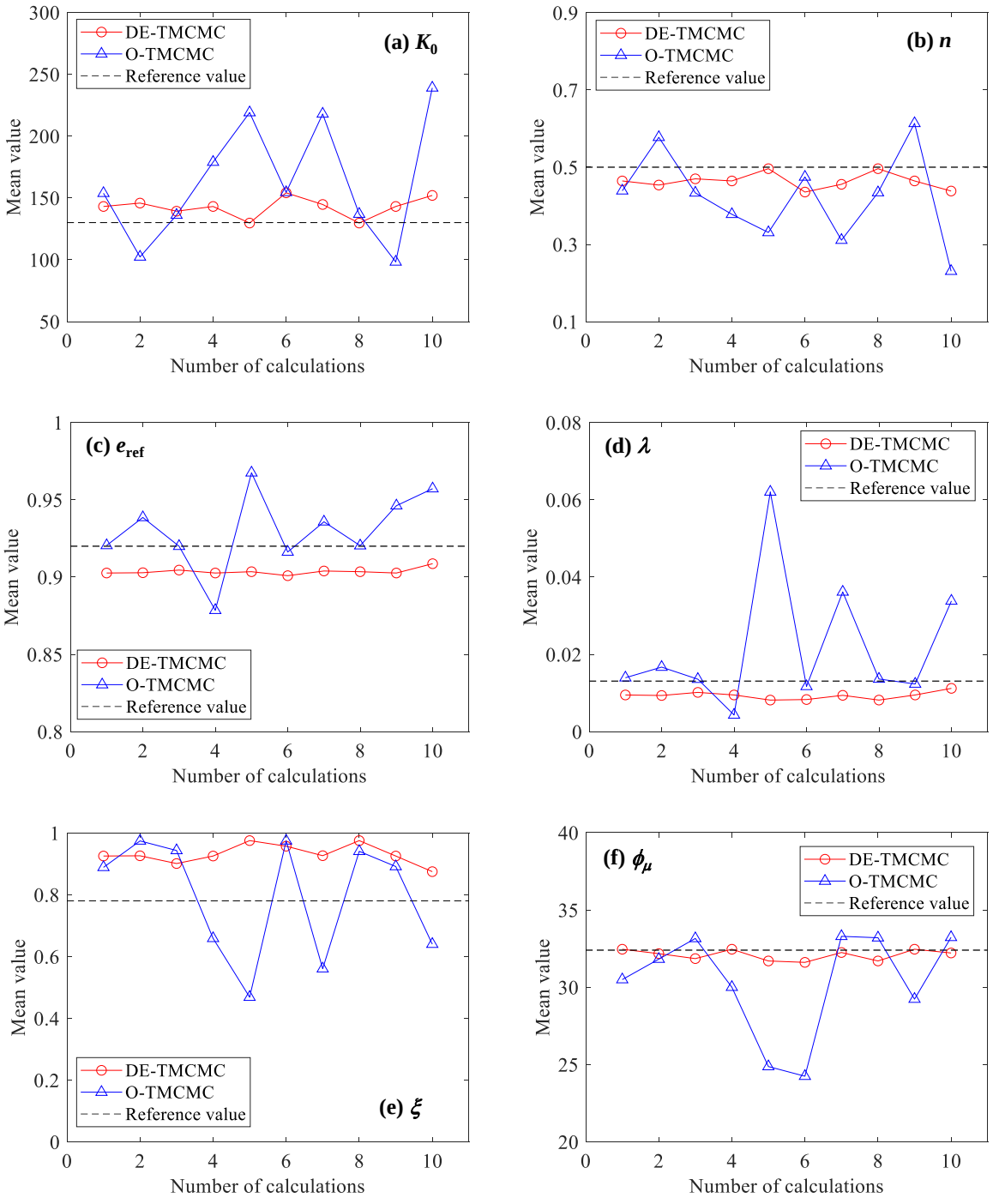
(a) K_0
(b) n
(c) e_{ref}
(d) λ
(e) ξ
(f) ϕ_μ
DE-TMCMC
O-TMCMC
Reference value
Mean value
Number of calculations

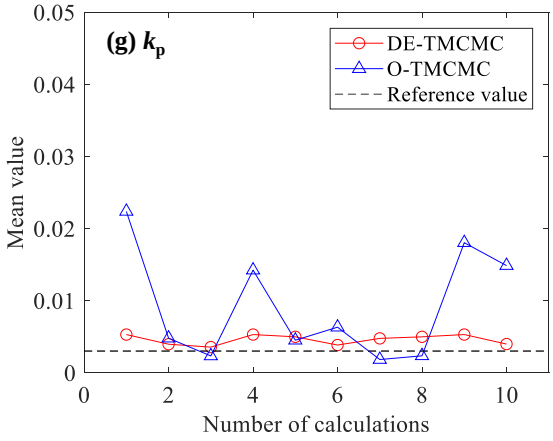
(g) k_p
DE-TMCMC
O-TMCMC
Reference value
Mean value
Number of calculations

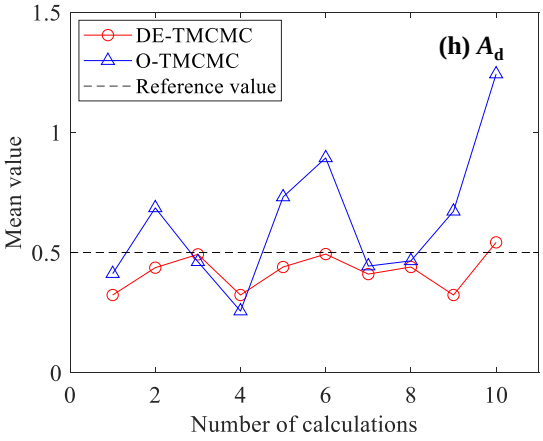
(h) A_d
DE-TMCMC
O-TMCMC
Reference value
Mean value
Number of calculations

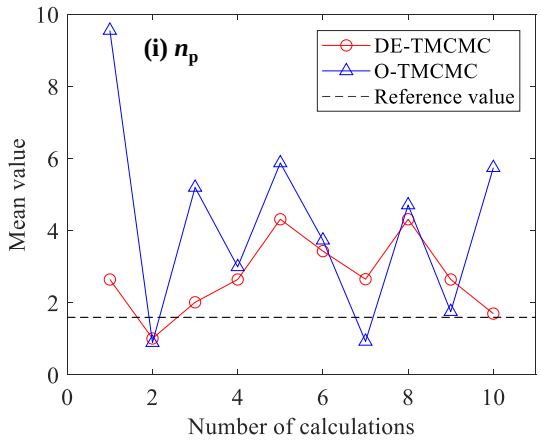
(i) n_p
DE-TMCMC
O-TMCMC
Reference value
Mean value
Number of calculations

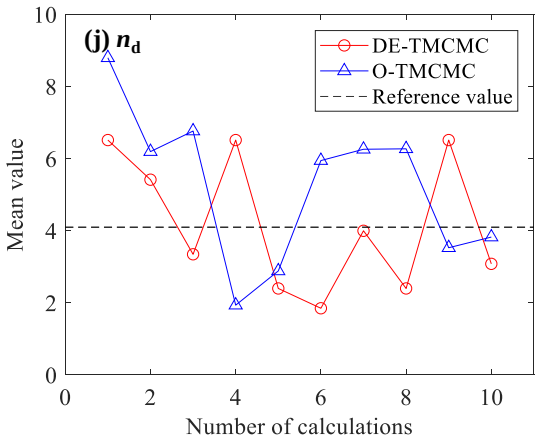
(j) n_d
DE-TMCMC
O-TMCMC
Reference value
Mean value
Number of calculations

Figure 9

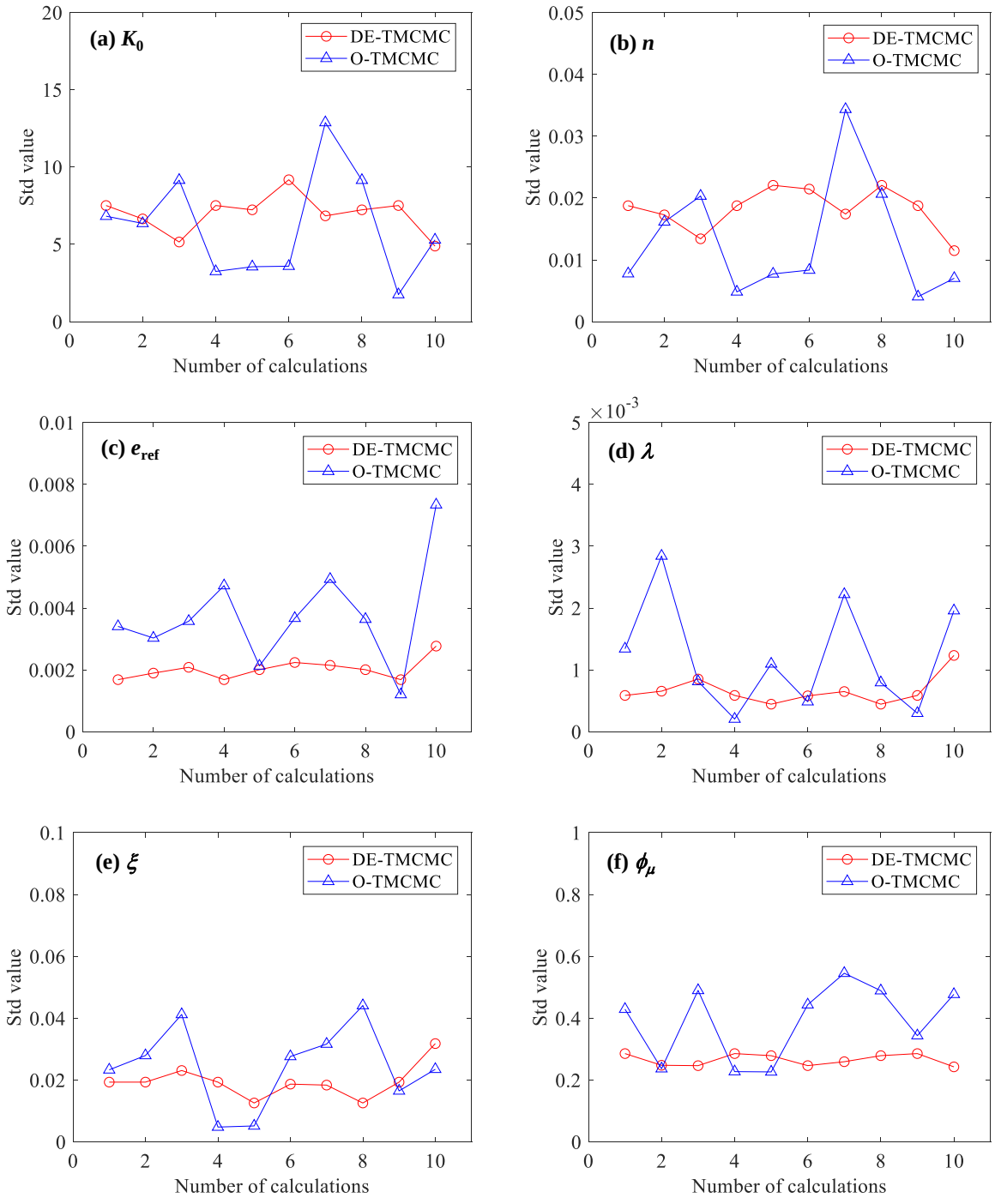
(a) K_0
DE-TMCMC
O-TMCMC
Std value
Number of calculations
(b) n
DE-TMCMC
O-TMCMC
Std value
Number of calculations
(c) e_{ref}
DE-TMCMC
O-TMCMC
Std value
Number of calculations
(d) λ
$\times 10^{-3}$
DE-TMCMC
O-TMCMC
Std value
Number of calculations
(e) ξ
DE-TMCMC
O-TMCMC
Std value
Number of calculations
(f) ϕ_μ
DE-TMCMC
O-TMCMC
Std value
Number of calculations

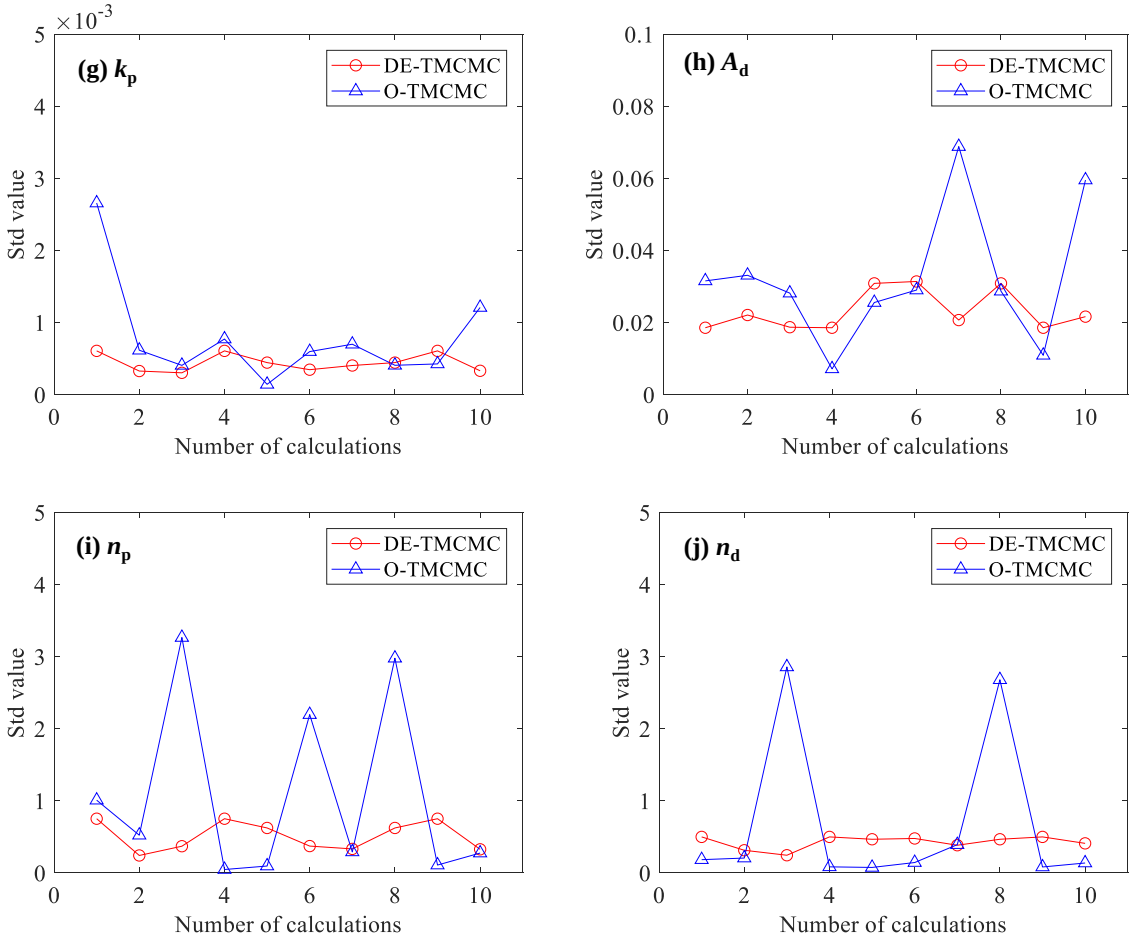
(g) k_p
DE-TMCMC
O-TMCMC
Std value
Number of calculations
(h) A_d
(i) n_p
(j) n_d

Figure 10

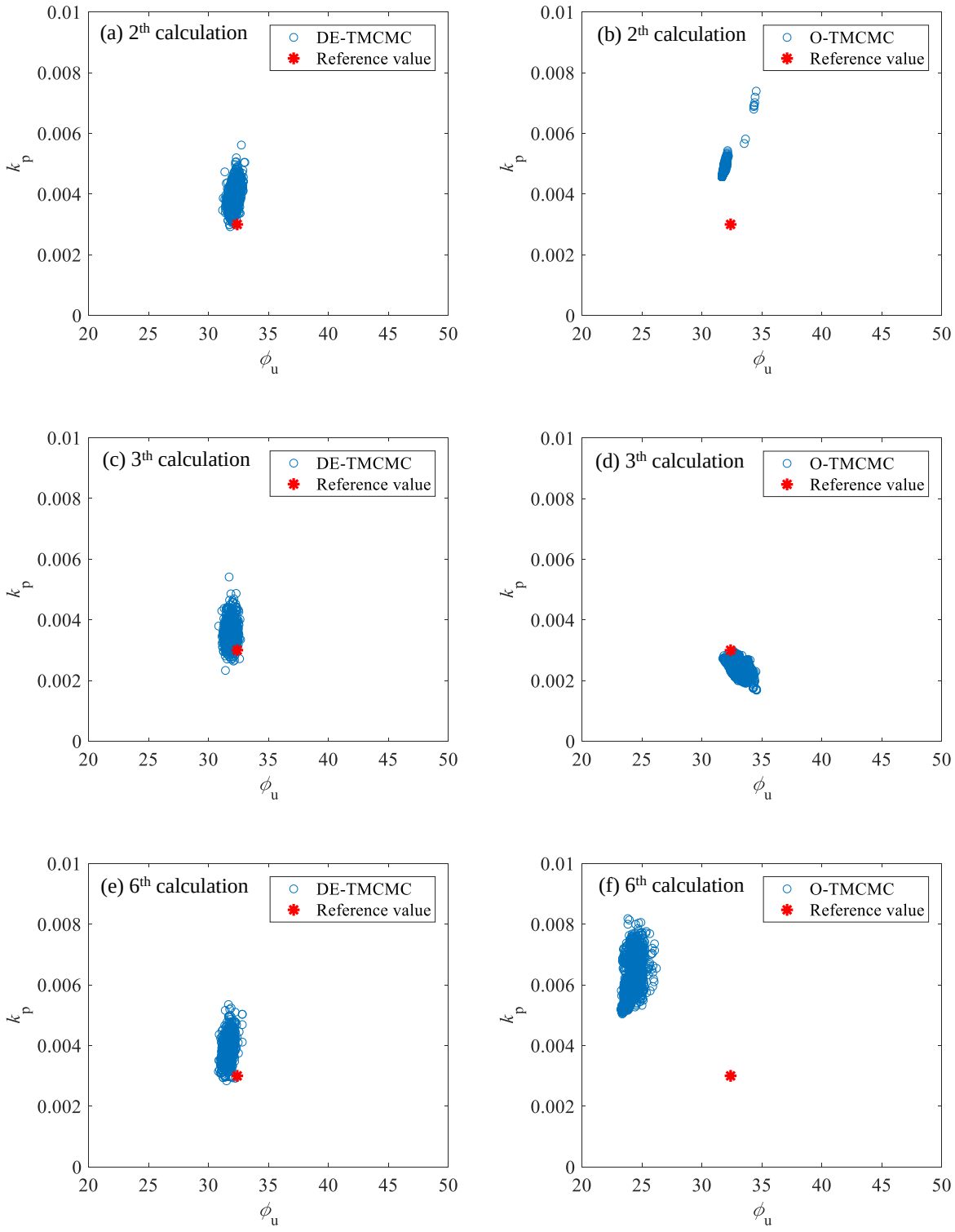
(a) 2th calculation
DE-TMCMC
Reference value
(b) 2th calculation
O-TMCMC
Reference value
(c) 3th calculation
DE-TMCMC
Reference value
(d) 3th calculation
O-TMCMC
Reference value
(e) 6th calculation
DE-TMCMC
Reference value
(f) 6th calculation
O-TMCMC
Reference value
k_p
ϕ_u
0.01
0.008
0.006
0.004
0.002
0
20
25
30
35
40
45
50

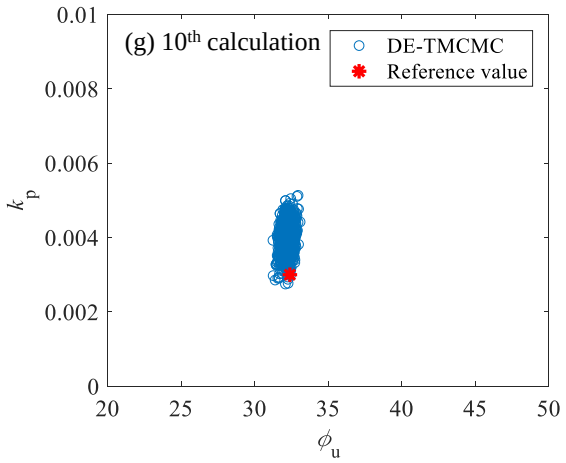
(g) 10th calculation
DE-TMCMC
Reference value
0.01
0.008
0.006
0.004
0.002
0
k_p
20
25
30
35
40
45
50
ϕ_u

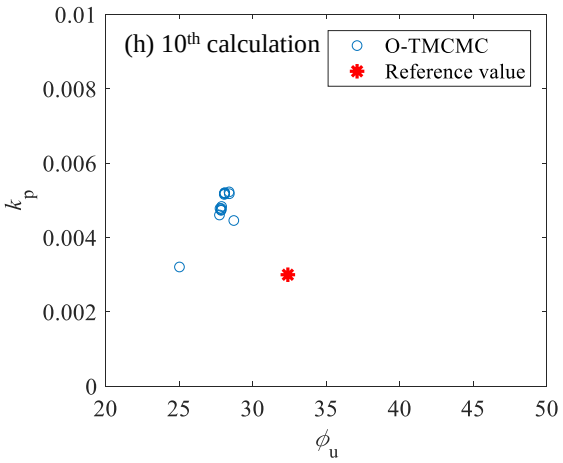
(h) 10th calculation
O-TMCMC
Reference value
0.01
0.008
0.006
0.004
0.002
0
k_p
20
25
30
35
40
45
50
ϕ_u

Figure 11

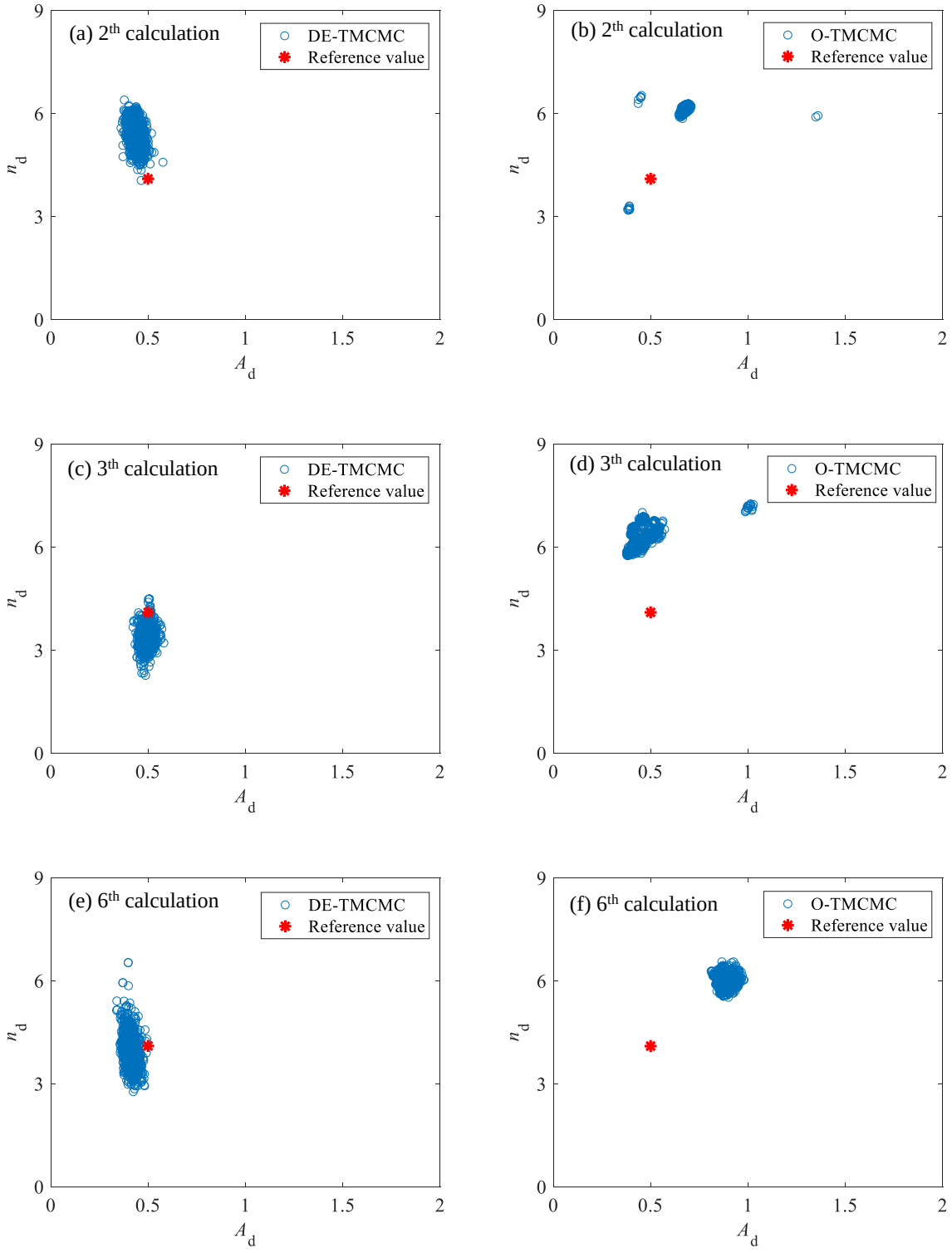
(a) 2th calculation
DE-TMCMC
Reference value
(b) 2th calculation
O-TMCMC
Reference value
(c) 3th calculation
DE-TMCMC
Reference value
(d) 3th calculation
O-TMCMC
Reference value
(e) 6th calculation
DE-TMCMC
Reference value
(f) 6th calculation
O-TMCMC
Reference value
n_d
A_d
0
3
6
9
0
0.5
1
1.5
2

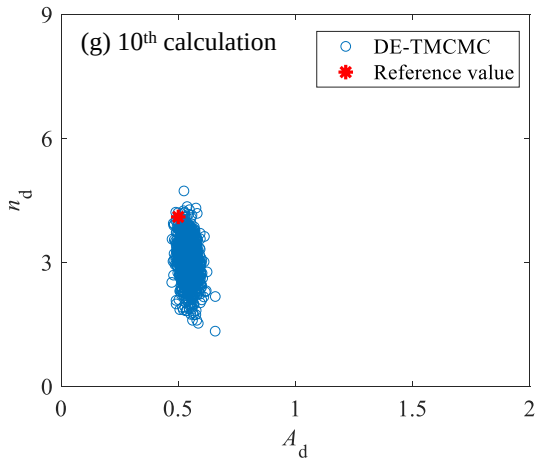
(g) 10th calculation
DE-TMCMC
Reference value
n_d
A_d
0
3
6
9
0
0.5
1
1.5
2

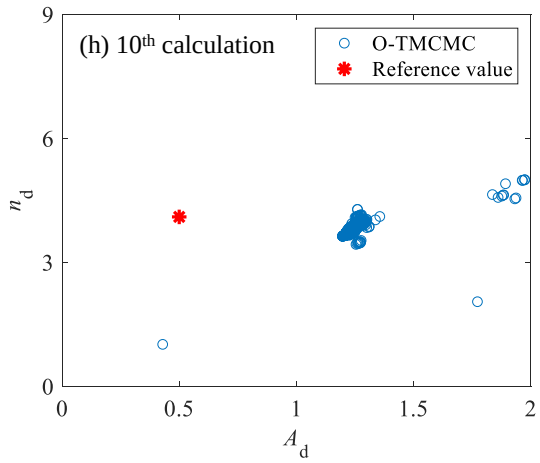
(h) 10th calculation
O-TMCMC
Reference value
n_d
A_d
0
3
6
9
0
0.5
1
1.5
2

Figure 12

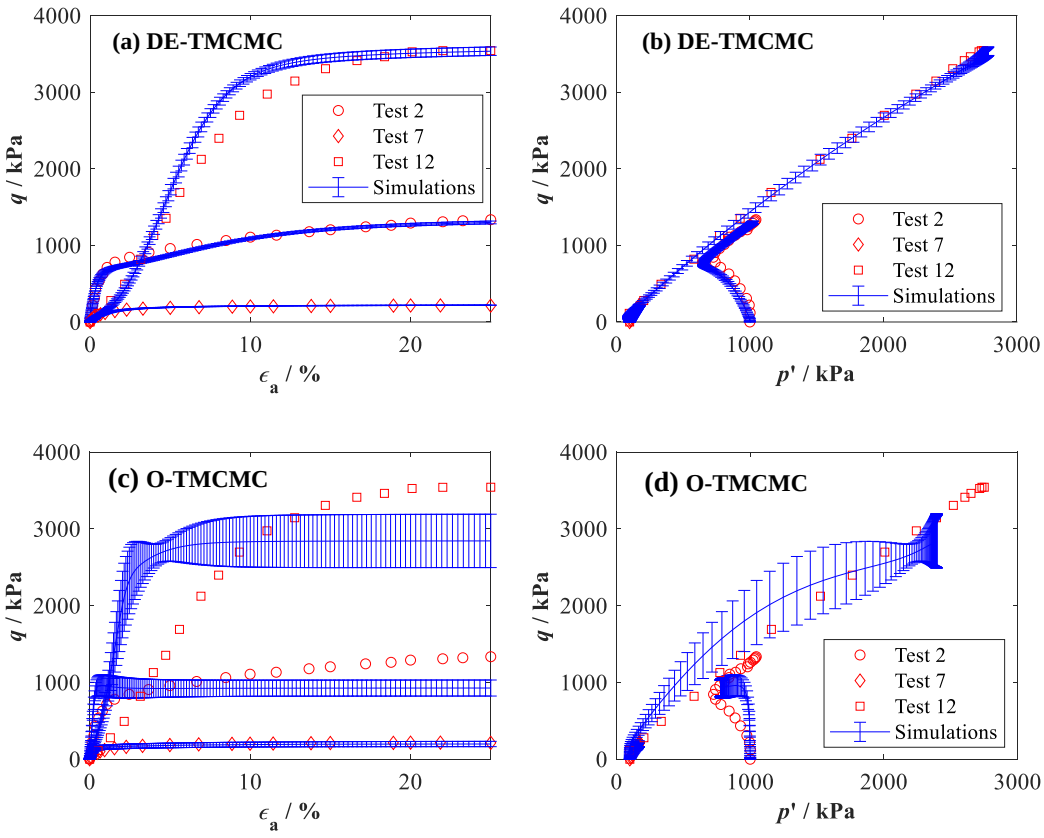
(a) DE-TMCMC
(b) DE-TMCMC
(c) O-TMCMC
(d) O-TMCMC
Test 2
Test 7
Test 12
Simulations
q / kPa
p' / kPa
ϵa / %
0
1000
2000
3000
4000
10
20

Figure 13

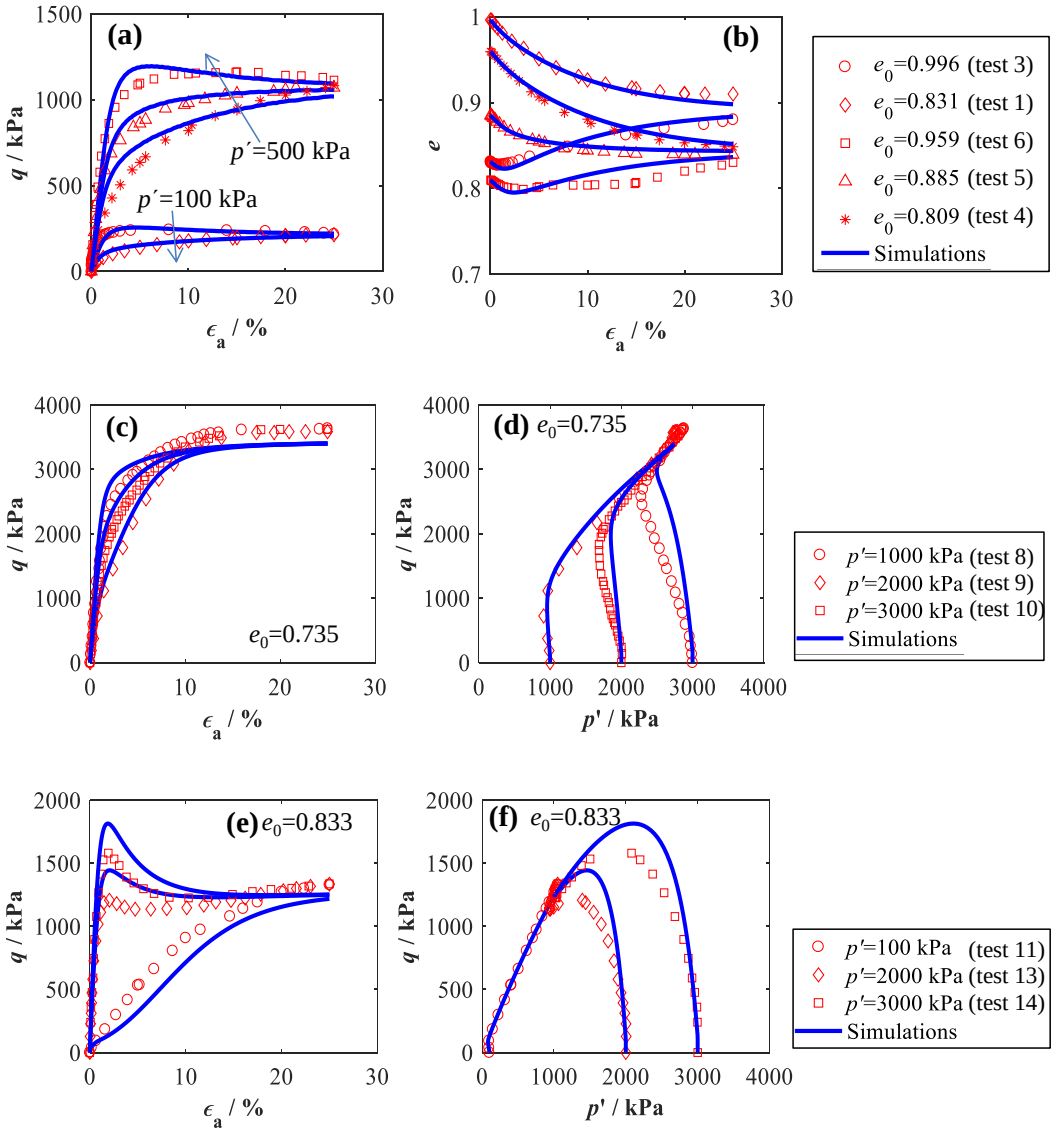
(a)
(b)
(c)
(d) e_0=0.735
(e) e_0=0.833
(f) e_0=0.833
q / kPa
e
ϵ_a / %
p' / kPa
p´=500 kPa
p´=100 kPa
e_0=0.735
e_0=0.996 (test 3)
e_0=0.831 (test 1)
e_0=0.959 (test 6)
e_0=0.885 (test 5)
e_0=0.809 (test 4)
Simulations
p'=1000 kPa (test 8)
p'=2000 kPa (test 9)
p'=3000 kPa (test 10)
p'=100 kPa (test 11)
p'=2000 kPa (test 13)
p'=3000 kPa (test 14)

Figure 14

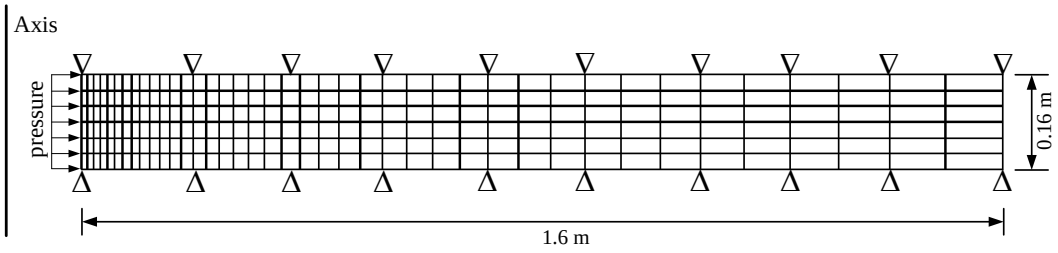

Figure 15

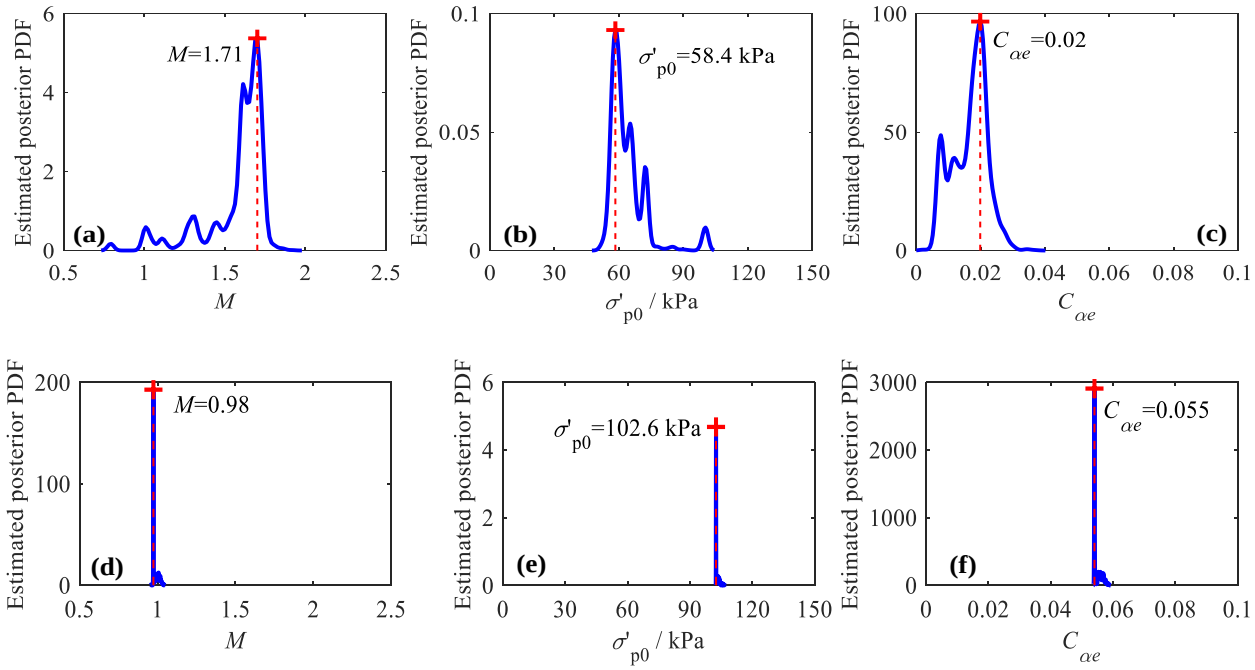
Estimated posterior PDF
M=1.71
(a)
M
σ'p0=58.4 kPa
(b)
σ'p0 / kPa
Cαe=0.02
(c)
Cαe
M=0.98
(d)
M
σ'p0=102.6 kPa
(e)
σ'p0 / kPa
Cαe=0.055
(f)
Cαe

Figure 16

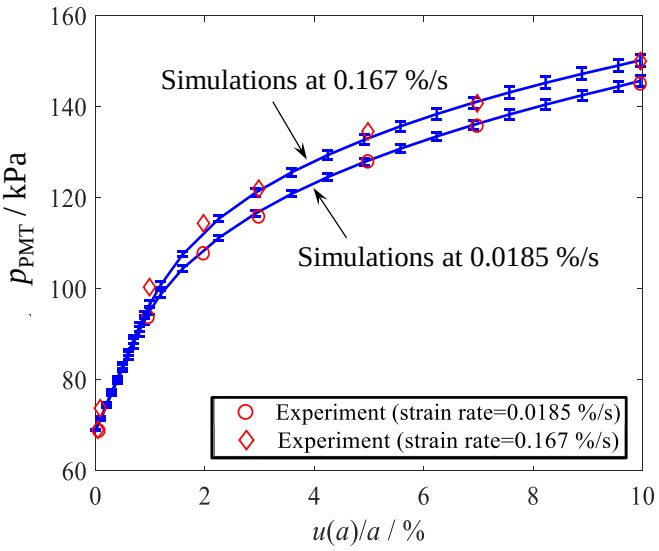
160
140
120
100
80
60
0
2
4
6
8
10
p_{PMT} / kPa
$u(a)/a$ / %
Simulations at 0.167 %/s
Simulations at 0.0185 %/s
Experiment (strain rate=0.0185 %/s)
Experiment (strain rate=0.167 %/s)